MAX-PLANCK-INSTITUT FÜR PLASMAPHYSIK

GARCHING BEI MÜNCHEN

Slow-Wave Coupling to the Lower-Hybrid Resonance

S. Puri, M. Tutter

IPP IV/59 July 1973

Die nachstehende Arbeit wurde im Rahmen des Vertrages zwischen dem Max-Planck-Institut für Plasmaphysik und der Europäischen Atomgemeinschaft über die Zusammenarbeit auf dem Gebiete der Plasmaphysik durchgeführt.

IPP IV/59 S. Puri
M. Tutter

Slow-Wave Coupling to the Lower-Hybrid Resonance

July 1973 (in English)

Abstract

Previously we have shown that in a cold, inhomogeneous, magnetized plasma half-space, the lower-hybrid resonance is accessible to the transverse-magnetic (TM) plane waves incident on the vacuum-plasma interface at an approximately grazing incidence, provided that at the hybrid layer $\omega_{pe}/\omega_{ce} \lesssim 0.4$. In this paper these results are extended to the slow-wave case when n_z, the refractive index in the static magnetic field direction exceeds unity. It is found that the plasma is indeed accessible to the slow waves if Golant's accessibility criterion $n_z > 1 + (\omega_{pe}/\omega_{ce})^2$ is satisfied, even though the computed plasma surface impedance is in wide variance with the Golant's results. The following recommendations can be made for coupling rf energy to the lower-hybrid resonance: (i) if $\omega_{pe}/\omega_{ce} \lesssim 0.4$, efficient coupling is possible by launching TEM-like waves on the plasma column, (ii) if $\omega_{pe}/\omega_{ce} \gtrsim 0.4$ and if the transverse machine dimensions exceed the rf vacuum wavelength, it is possible to couple TM waves using passive slow-wave structures inside the machine walls, (iii) if $\omega_{pe}/\omega_{ce} \gtrsim 0.4$, but for smaller machine

dimensions, recourse must be taken to transverse-electric slow-wave coupling with current carrying coils of appropriate periodicity. We note parenthetically that if, as pointed out by Glagolev, propagation from the plasma edge till the hybrid layer is not materially affected by the inclusion of finite temperature effects, by far the most elegant solution (with potential application to thermonuclear plasmas) for coupling rf energy from the second till the twentieth ion-cyclotron harmonic waves is by launching TEM-like waves in the coaxial waveguide formed by the plasma column and the containing walls.

I. Introduction

In previous publications[1,2] we have shown that in a cold, inhomogeneous, magnetized plasma half-space, the lower hybrid resonance is accessible to the transverse-magnetic (TM) plane waves incident on the vacuum-plasma interface at an approximately grazing incidence ($n_z \lesssim 1$) provided that at the hybrid layer $\omega_{pe}/\omega_{ce} \lesssim 0.4$. These results are in conflict with the existing accessibility criteria which invariably require that n_z, the refractive index in the static magnetic field direction to exceed unity for possible coupling of rf energy to the hybrid resonance. The principal attraction of the above findings is that at least for the restricted parameter range of ω_{pe}/ω_{ce}, they open up the possibility of coupling without the cumbersome intrusion of a slow-wave device. As an example, the coupling problem in the MIT Alcator machine[3] will be considerably alleviated if the waveguide is oriented to launch a TEM-like wave on the coaxial system composed of the plasma column and the torus walls.[2]

Nevertheless, since for several laboratory plasmas ω_{pe}/ω_{ce} may have appreciably larger values, we extend the above calculations to the case $n_z > 1$ in this paper. This would also provide us with the opportunity of directly comparing our results with the existing analytical solutions.

Several difficulties are encountered in the evaluation of the slow-wave coupling efficacy. Unlike the case $n_z < 1$,

for the slow-wave case $n_z > 1$ it is not possible to distinguish between the incident and the reflected waves and the concept of transmission co-efficient is not applicable. We shall content ourselves with comparing the energy coupled into the plasma for a given excitation of the slow-wave structure to that coupled into a slab of stainless steel for identical excitation conditions. This comparison is an indication of the relative energy absorbed in the plasma and the machine walls and is, therefore, a measure of coupling efficiency. Another important quantity computed is the plasma surface impedance $\sigma_s = E_{tang}/H_{tang}$ which would facilitate the design of the slow-wave structure itself.

In Sec. II the models used for the computations is described. A brief review of the theory is given in Sec. III. In Sec. IV transmission into the plasma and stainless steel is compared for several values of ω_{pe}/ω_{ce} as a function of n_z. Detailed calculations for the representative case with $\omega_{pe}/\omega_{ce} = 0.57$ and $n_z = 1.5$ are presented in Sec. V followed by a discussion of the results in Sec. VI. The method for the practical realization of the slow-wave structure for TM excitation is discussed in Appendix A.

II. The Model Used

The model used in the computations with TE excitation is shown in Fig. 1. The plasma half-space extends from $x = o$ to $x = \infty$ and the static magnetic field is along the z-direction. The slow-wave TE antenna situated at the $x = -b$

consists of a current sheet with the surface current density $J_s = J_{oE} \exp i (k_z z - \omega t)$ along the y-direction. Throughout this paper b = g = 1 cm and the normalization J_{oE} = 1 ampere/cm is used. The boundary conditions at x = -b envisage the comtinuity of E_y, E_z and H_y while H_z has a discontinuous jump due to the surface current J_s.

For the TM excitation the current sheet is replaced by a fictitious magnetic current of amplitude J_{oM} = 1 Weber/sec-cm so that E_z suffers a discontinuity at x = -b. Whereas the TE excitation may be readily approximated by a "Stix coil", the practical realization of the TM excitation requires a slow-wave structure described in Appendix A. The slow-wave structure, however, at best only roughly recreates the field configuration of the idealized TM antenna carrying a magnetic current. The usage of the concept of a magnetic current is by no means unduly esoteric. It is in fact possible to construct a consistent theory of electromagnetism postulating the existence of free magnetic charges.[4]

All field quantities are assumed to possess space and time dependence exp i $(k_x x + k_z z - \omega t)$ with no variation in the y-direction. The density profile is taken into account using a stratified plasma model. The absorption mechanism considered is the momentum transfer collisions between the electrons and the ions using the Langevin model. The full cold-plasma dielectric tensor used in a plasma slab of uniform electron density n_e is,

$$K = \begin{pmatrix} K_\perp & -iK_x & 0 \\ iK_x & K_\perp & 0 \\ 0 & 0 & K_\parallel \end{pmatrix} \qquad (2.1)$$

where

$$K_\perp = 1 - \frac{\omega_{pi}^2}{\omega^2 - \omega_{ci}^2} - \frac{\omega_{pe}^2}{\omega^2 - \omega_{ce}^2} \qquad (2.2)$$

$$K_x = \frac{\omega_{ci}}{\omega} \frac{\omega_{pi}^2}{\omega^2 - \omega_{ci}^2} - \frac{\omega_{ce}}{\omega} \frac{\omega_{pe}^2}{\omega^2 - \omega_{ce}^2} \qquad (2.3)$$

$$K_\parallel = 1 - \frac{\omega_{pi}^2}{\omega^2} - \frac{\omega_{pe}^2}{\omega^2} \qquad (2.4)$$

$\omega_{pi}^2 = n_e e^2/M\epsilon_o$, $\omega_{pe}^2 = n_e e^2/m_\nu \epsilon_o$, $\omega_{ci} = eB_o/M$ and $\omega_{ce} = eB_o/m_\nu$. In conformity with the use of the Langevin equation, m_ν in the above equations is defined as

$$m_\nu = m\,(1 + i\,\nu_{ei}/\omega) \qquad (2.5)$$

where m is the electron mass and ν_{ei} is the electron-ion momentum transfer collision frequency according to Spitzer[5]. We shall sometimes specify ν_{ei} by the equivalent temperature T. This results in a variable value of ν_{ei} across the inhomogeneous plasma column. It should, however, be borne in mind

that, apart from specifying ν_{ei}, T does not imply any departure from the cold-plasma theory. The mean value of ν_{ei} averaged in the region $o < x < g$ will be denoted by $\langle \nu_{ei} \rangle$. Throughout the present computations, T is chosen so as to make $\langle \nu_{ei} \rangle / \omega = 10^{-2}$.

The plasma density is assumed to rise linearly from $n_e = 0$ to $n_e = n_{max}$ as x increases from x = 0 to x = g and thereafter remains constant as shown in Fig. 1. The maximum plasma density is invariably chosen so that $n_{max} = 1.3\, n_{1h}$ where n_{1h} is the density corresponding to the lower-hybrid resonance. The region $0 < x < g$ is stratified into 99 slabs, while $x > g$ forms the 100th slab.

Defining $\tilde{K}_\perp = K_\perp - n_z^2$, the dispersion relation can be written as

$$n_x^2 = \frac{K_\perp \tilde{K}_\perp - K_x^2 + K_{\parallel} \tilde{K}_\perp}{2 K_\perp} \pm \left[\left(\frac{K_\perp \tilde{K}_\perp - K_x^2 + K_{\parallel} \tilde{K}_\perp}{2 K_\perp} \right)^2 + \frac{K_{\parallel}}{K_\perp} \left(K_x^2 - \tilde{K}_\perp^2 \right) \right]^{1/2} \qquad (2.6)$$

Corresponding to the four roots of this equation, the x-components of the electric fields associated with the four waves in a given plasma slab are

$$E_{x\pm}^{f,s} = \hat{E}_{x\pm}^{f,s} \exp i \left(k_{x\pm}^{f,s} x + k_z z - \omega t \right) \qquad (2.7)$$

while E_y, E_z, H_x, H_y and H_z may be expressed in terms of E_x using the dielectric tensor and the Maxwell equations. The indices f (fast) and s (slow) correspond respectively to the smaller and the larger roots of n_x^2. For each of the roots n_x^2, the two waves associated with $\pm n_x$ are labelled plus and

minus respectively so that $n_{x+} = - n_{x-}$. The slow wave is the quasi-extraordinary mode which encounters the resonance at the lower-hybrid layer as $K_\perp \to 0$. In the slab to the right of $x = g$, there are only two waves, one fast and one slow, each of which decays for increasing x, there being no sources at infinity.

In the vacuum region $-b < x < 0$ between the current sheet and the plasma boundary there are in general four waves, two TE and two TM, while in the region $x < -b$ to the left of the current sheet there are only two waves, one TE and one TM, each of which decays for decreasing x.

Apart from these modifications, the computational procedure and checks are the same as described in Ref. 2. The gas used in all the computations is Deuterium and the static magnetic field $B_o = 100$ kG ($f_{ci} = 76$ MHz).

III. Brief Review of the Theory

For optimum transmission it is clearly desirable that n_x, the refractive index in the direction of the density gradient be real everywhere between the antenna and the resonant layer. From an analysis of the cold-plasma dispersion relation (2.6), Stix[6] concluded that the condition for propagation is satisfied (except in a narrow region of inconsequential importance near the plasma edge) if

$$n_z > 2 \left(1 + \omega_{pe}^2 / \omega_{ce}^2\right) \qquad (3.1)$$

where n_z is the refractive index along the static magnetic field direction z. Through certain algebraic improvements, Parker[3] and Golant[7], respectively, arrive at the following less stringent variations of the propagation condition,

$$n_z > 1 + \omega_{pe}/\omega_{ce} \tag{3.2}$$

and

$$n_z > 1 + \omega_{pe}^2/\omega_{ce}^2 \tag{3.3}$$

The methods suggested for obtaining the required longitudinal retardation include the Stix coil [6], "gap excitation"[3] or a "slow-wave structure"[7,8].

With this provision one may anticipate using the WKB theory that the wave propagates without reflection provided that the refractive index is a slowly varying function of position. Although valid in the intermediate region, this so-called adiabaticity condition is severely strained both at the vacuum-plasma interface and near the resonant layer in the interior of the plasma. Using singular turning point analysis, Budden[9] and Stix[6] have shown that the wave propagates in the intermediate region to the hybrid layer and is completely absorbed without reflection.

However, the analytical treatments of the crucial question of a possible mismatch at the vacuum plasma interface remain entirely unconvincing. The problem has been treated in almost

identical manners by Parker[3] and Golant[7]. Paradoxically, in their analysis, the thin evanescent region near the plasma edge which was considered inconsequential by Stix[6], assumes critical importance. Apart from using this questionable model, they both seem to err in neglecting the E_z' term in comparison with the E_z term in the differential equation for the electric field[10]. This oversight, in itself, would render their calculations of the plasma impedance incorrect.

Although the impedance results must await the solution of the complete boundary value problem, the extent to which the propagation conditions (3.1 - 3.3) are valid can be readily ascertained from the dispersion relation (2.6). The solid curve in Fig. 2 shows the critical value of n_z above which n_x becomes real between the plasma edge and the hybrid layer (except the thin region mentioned already). To obtain this curve, n_x was numerically computed using (2.6) for several values of $(\omega_{pe}/\omega_{ce})$ and the boundary between regions of propagation and evanescence was determined. The emperical relation obtained for the propagation condition from this curve is

$$n_z > 1 + 0.4\,(\omega_{pe}^2/\omega_{ce}^2) \qquad (3.4)$$

and is most closely approximated by the analytical form given be Golant[7] which, along with the propagation conditions of Stix[6] and Parker[3] is sketched in Fig. 2. Detailed dispersion relations for several n_z and for three different values of ω_{pe}/ω_{ce} are shown in Figs. 3 - 5. The unprimed curves are for the collisionless case, while for the primed curves $\langle \nu_{ei} \rangle \sim 10^{-2}$.

IV. Coupling Efficiency and Surface Impedance

The power coupled into the plasma is given by the x-component of the Poynting vector $P_x = 1/2\ \mathrm{Re}\ (E \times H^*)_x$ at the plasma surface x = 0. For the case of TM excitation, P_x plotted as a function of n_z for five different values (see Table I) of ω_{pe}/ω_{ce} is shown in Fig. 6a. Over 80% of the total power coupled goes into exciting the slow-wave, which is completely absorbed at the lower-hybrid layer. The large black dots on these curves correspond to the value of n_z given by (3.4) when the propagation condition is fulfilled. There is a distinct improvement in the coupling efficiency when n_z exceeds this critical value. The gradual roll-off in P_x for increasing n_z is due to the increased evanescence of the wave from the antenna till the plasma edge. The same effect is responsible for improved coupling for smaller values of n_z when the propagation condition is not fulfilled. The five dashed curves in Fig. 6a show the power absorbed in a stainless steel half-space substituted for the plasma under identical conditions of excitation. It is gratifying to note that if the propagation condition is fulfilled, the power coupled into the plasma exceeds that in the steel typically by three orders of magnitude. Allowing for a tenfold increase in the losses occurring in an actual slow-wave structure, we may still hope to achieve high coupling efficiencies in a practical device.

The surface impedance $\sigma_s = -E_z/H_y$ of the plasma half-space for the TM excitation is shown in Fig. 6b. Since σ_s is independent of antenna placement and excitation strength, these

curves possess a more general significance and could be used for designing the coupling structure itself. The surface impedance is highly capacitive and under conditions of efficient coupling, the resistive component of σ_s is typically 10 Ω. This value of surface resistance is at least two orders of magnitude greater than the value given by Golant[11]. We can also use these results for estimating the resistive impedance presented to a waveguide flush mounted on the machine wall with its small dimension parallel to the magnetic field, the so-called "gap excitation" in the Alcator[3]. Neglecting end effects and using the parameters $\omega_{pe}/\omega_{ce} = 0.17$ and $n_z = 1.1$, the computed value of $Re(\sigma_s) \sim 10\,\Omega$ so that the resistive impedance seen by the waveguide, assuming that the ratio of the larger to the smaller dimension is 2, is roughly 5 Ω. In principle, it is feasible to create a match between the waveguide (typical impedance $> 377\,\Omega$) and the plasma using stub tuners. For this case, however, as was pointed out in Ref. 2, it may be more logical to use the waveguide as a TEM antenna with its axis along the magnetic field direction and the small dimension perpendicular to the plasma surface.

Similar curves for the coupled power and the surface impedance defined by $\sigma_s = E_y/H_z$ for TE excitation are shown in Fig. 7. Once again it is seen that the power coupled into the plasma exceeds that coupled into steel by three orders of magnitude. However, only 10% of this power goes into exciting the slow wave, the rest going into the fast wave which would not nominally contribute towards energy absorption. Allowing for an order of magnitude increase in copper losses in an

actual machine, this method of coupling may still prove valuable when the machine dimensions are not large enough to accommodate the slow-wave structure. The surface impedance, in this case, is inductive and the resistive component is of the order of 30 Ω under conditions of coupling.

V. Detailed Results for a Representative Case

We shall now describe detailed results for electric field, Poynting vector, energy and group velocities for a particular case with $n_z = 1.5$ and $\omega_{pe}/\omega_{ce} = 0.57$, both for the TM and TE excitations. The propagation constant for this case is shown in Fig. 4b and is real everywhere between the plasma edge and the hybrid layer except for a narrow region of width Δ near the plasma edge (not shown in the figure). The thickness $\Delta \sim O\left[(m/M)h\right]$, where h is the distance of the hybrid layer from the plasma edge. For the parameters of this paper Δ is less than one-hundredth of a millimeter.

The x-component of the electric field amplitude of the fast and the slow waves, both for the TM and TE polarizations is shown in Fig. 8. While the slow-wave field increases to a maximum near the hybrid layer, the fast wave propagates oblivious of the resonance. The phases of these waves are plotted in Fig. 9. The vertical scale is to be read with the positive sign for the fast wave and the negative sign for the slow wave. Since the energy and hence the group velocity is transported along the x-direction, the decreasing phase angle of the slow

wave points to its backward character between the plasma edge and the hybrid layer.

The amplitude and phase of the total transverse electric field (the quantity actually observed in an experiment) are shown in Fig. 10 and Fig. 11 for the case of TM and TE excitation, respectively. The interference pattern between the backward (slow) and the forward (fast) waves is clearly visible. The comparatively stronger excitation of the fast wave for the TE excitation results in a stronger modulation of the slow wave field. The combined wave possesses a backward character between the plasma edge and the hybrid layer.

The electric field configuration in the x-z plane for the TM excitation is shown in Fig. 12. The large electron conductivity in the magnetic field direction causes the electric lines of force to be nearly normal to the plasma surface. Therefore, it would be incorrect to assume that the tangential component E_z of the electric field imposed by the antenna will not be altered by the presence of the plasma[3]. Inside the plasma, the wave becomes electrostatic and the electric field is approximately normal to the nodal planes as shown in the figure. The wavelength decreases as the hybrid resonance is approached and thereafter increases due to the presence of the fast wave alone.

In a similar manner, the magnetic field configuration in the x-z plane with the TE excitation is shown in Fig. 13.

The Poynting vector components P_x, P_y and P_z for the case of TM excitation are shown as a function of x in Fig. 14. Due to the cubic compression of the vertical scale, there is a de-emphasis in contrast of the amplitude. The x-component of the Poynting vector P_x is well behaved with a predictable drop (80%) at the hybrid layer, implying that 80% of the total energy coupled into the plasma goes into the excitation of the slow wave. The remaining two components of the Poynting vector P_y and P_z, on the other hand, exhibit rather peculiar and hitherto unsuspected behaviour. They are both of an oscillatory nature and the phase of P_z leads that of P_y by an angle $\pi/2$. As a result, the Poynting vector follows a counterclockwise path in the x-z plane (Fig.15). In Fig. 15 the values of x are marked along the P_y - P_z curve.

Similar curves for the TE excitation are shown in Figs. 16 and 17. Since for this case P_z has larger excursions in the negative side, the projection of P_y - P_z more nearly encircles the origin.

The foregoing observation that there is a component of P_y comparable to P_z (or P_x), even though the dispersion relation (2.6) does not make the existence of a group velocity component in the y-direction explicitly obvious, points out the necessity to differentiate between the group velocity $v_g = \partial\omega/\partial k$ and the energy velocity v_E defined as the quotient of Poynting vector and energy density. The group velocity and the energy velocity components both for the TM and TE excitation are shown in Fig. 18. It is clear from these figures that the actual correlation between the direction of energy flow and the calculated group velocity in the present case of an inhomogeneous

medium is none too strong. In Fig. 18, note that both for the TM and TE excitations, the energy velocity beyond the hybrid layer assumes identical values. This is due to the presence of the fast wave alone in this region.

Based on the concept of energy velocity, we may attempt to visualize the propagation of an energy pulse from the plasma edge into the interior of the plasma assuming that the pulse travels with the energy velocity. Figures 19 and 20 show a three-dimensional representation of pulse propagation for the TM and TE excitations, respectively. As the pulse travels in the x-z plane, it has a snaking motion along the y-axis. Since the TM wave dominantly excites the slow wave, it takes longer (28 nsec) to arrive at the hybrid layer as compared to the TE case (4 nsec). Furthermore, for the TE excitation, there is a stronger tendency for the pulse to wander to and fro in the z-direction; as a result the energy remains more localized than for the TM case when the pulse travels a long distance in the z-direction before encountering the hybrid resonance. If cylindrical, instead of planar, geometry were to be considered, then even for the m = 0 mode, the energy coupled at the plasma surface would tend to wrap itself around the plasma column as it went inwards and along the column direction.

VI. Discussion

Together with the complementary work of Ref. 2, this paper removes most of the speculation concerning the accessibility to the lower-hybrid resonance and brings us closer to a complete

understanding of this important problem. Accessibility to the lower-hybrid resonance may have an important bearing on the heating of thermonuclear plasmas using ion-cyclotron harmonic waves if, as pointed out by Glagolev[12], propagation from the plasma edge till the hybrid layer is not materially affected by the inclusion of finite temperature effects.

In Ref. 2 it was shown that for a large class of physically interesting cases ($\omega/\omega_{ci} \lesssim 20$) it was possible to obtain penetration for $n_z < 1$, so that coupling can be achieved in a simple manner without the erection of additional coils or structures inside the vacuum vessel. The present results show that for the case $\omega/\omega_{ci} \gtrsim 20$, it becomes imperative to use a slow-wave structure. For transverse machine dimensions exceeding the rf wavelength, it is possible to obtain TM wave coupling by using passive slow-wave structures, while for smaller machine dimensions recourse must be taken to current carrying coils. We reiterate, however, that if Glagolev's assertion is true, the most elegant solution for coupling rf energy from the second till the twentieth ion-cyclotron harmonic waves in a hot plasma is through using an antenna launching TEM-like modes on the co-axial plasma waveguide.[2]

Of the several accessibility criteria obtained from analytical considerations, that due to Golant[7] most closely resembles our findings (see Fig. 2), even though the computed plasma surface impedance is in wide variance with Golant's results. The grounds for this disagreement are, as already pointed out, presumably the use of a suspect model as well as an erroneous

algebraic treatment in Golant's approach.

For the case of slow waves, it is not possible to distinguish between the incident and the reflected waves, all accessibility estimates are made by an indirect comparison of coupled power into stainless steel. The present analysis, therefore, is unable to expose the extent of the validity of the WKB approximation. Yet in the light of considerably better coupling into the plasma as compared with stainless steel, one may confidently recommend the use of slow-wave coupling if deemed unavoidable due to the existing parameter values.

A somewhat unexpected finding to emerge from this study is the blatant disagreement possible between the group and energy velocities. The energy appears to approach the hybrid resonance after considerable meanderings both along the y- and the z-directions.

In conclusion, we trust that this work would provide the guidelines for selecting the proper coupling configuration, in addition to suggesting possible measurements in an experiment designed for lower-hybrid resonance studies.

Acknowledgment

This work has been undertaken as part of the joint research program between the Max-Planck-Institut für Plasmaphysik and Euratom.

REFERENCES AND FOOTNOTES

1. S. Puri and M. Tutter, Z. Naturforsch. 28a, 438 [1973]

2. S. Puri and M. Tutter, Z. Naturforsch. (to be published); Further references on the topic are given in this reference.

3. R. Parker, QPR No. 102, Res. Lab. of Electronics, MIT, Cambridge, Mass. 97 [1971]

4. R. M. Fano, L. J. Chu and R. B. Adler, Electromagnetic Field Energy and Forces (John Wiley & Sons, New York, 1960)

5. L. Spitzer, Jr., Physics of Fully Ionized Gases (Interscience Publishers, New York, 1962)

6. T. H. Stix, Theory of Plasma Waves (McGraw Hill, New York, 1962)

7. V. E. Golant, Zh. Tekh. Fiz. 41, 2492 [1971]; Sov. Phys. Tech. Phys. 16, 1980 [1972]

8. Since in an actual reactor, the transverse dimensions of the apparatus would exceed the free-space wavelength of the rf source, Derfler has suggested (in the somewhat different context of enhancing Landau damping of Bernstein modes) coupling to the slow waves by constructing a slow-wave structure within the reactor walls (communicated to the "Advisory Group on Plasma Heating", Grenoble, March 29-31, 1971).

9. K. G. Budden, Proc. Roy. Soc. A227, 516 [1955]

10. From Ref. 3, p. 105, the differential equation for the electric field is

$$\frac{\partial^2 E_z}{\partial x^2} - \frac{K_\perp'}{K_\perp}\,\frac{n_z^2}{K_\perp - n_z^2}\,\frac{\partial E_z}{\partial x} + k_0^2\,\frac{K_{11}}{K_\perp}\left(K_\perp - n_z^2\right) E_z = 0$$

Near the plasma edge it is readily shown that the ratio ξ of the second to the last term is given by

$$\xi \sim O\left\{ \frac{\lambda_o}{2\pi h} \frac{n_z^2}{(1-n_z^2)^{3/2}} \right\},$$

where λ_o is the free-space wavelength of the rf field and h is the depth of the hybrid layer measured from the plasma edge. From this equation it is clear that the assumption $\xi << 1$ is not permissible in any case of practical interest.

11. Ref. 7, Eq. (38).

12. V. M. Glagolev, Plasma Phys. 14, 301 [1972]

Appendix A

Design Considerations for the Slow-Wave Structure

The magnetic current sheet for TM excitation is, in practice, approximated by a passive Millman line of the type shown in Fig. 21. It is our endeavor to show how to design an appropriate Millman line using the computed value of the plasma surface impedance

$$\sigma_s = -(E_z/H_y)_{x=0} \tag{A1}$$

given in Sec. III for various values of n_z and ω_{pe}/ω_{ce}.

We consider the propagation of a wave, of wavelength λ and wavenumber $k_{zo} = 2\pi/\lambda$, along the positive z-direction. The field configuration of the Millman line is necessarily more complex due to the presence of space harmonics. The field quantities satisfy the condition

$$F(z+L) = F(z)\exp(i\Psi) \tag{A2}$$

where $\Psi = \Psi_o + 2\pi\nu$, $\nu = 0, \pm 1, \pm 2, \ldots$

$$\Psi_o = k_{zo} L,$$

and L is the periodicity of the Millman line. The ν values other than zero stand for the space harmonics with the associated wavenumber

$$k_{z\nu} = k_{zo} + \frac{2\pi}{L}\nu. \tag{A3}$$

From the general relation

$$k_{z\nu}^2 + k_{x\nu}^2 = k_o^2 \qquad \text{(A4)}$$

where $k_o = \omega/c$, and using (A3) one obtains

$$k_{x\nu} = k_o \left[1 - \left(\frac{\lambda_o}{L}\right)\left(\nu + \frac{L}{\lambda}\right)^2\right]^{1/2},$$

where $\lambda_o = 2\pi/k_o$. For simplicity, we assume

$$|n_{z\nu}| = \frac{\lambda_o}{L}\left|\nu + \frac{L}{\lambda}\right| > 1$$

which implies $k_{x\nu}^2 < 0$. In a practical situation it is conceivable that the above assumption is invalidated, in which case a somewhat more involved analysis must replace the following treatment. For further discussion of this problem as well as for a more complete treatment of the Millman line including the existence of pass and stop bands, the reader is referred to W. Kleen and W. Ruppel, Arch. für Elektrotechnik 40, 280 [1952]. With this provision, the field components H_y and E_z in the region $-b \leq x \leq 0$, may be written as (the time dependence has been omitted),

$$H_y = \sum_{-\infty}^{\infty} (A_\nu \cosh \varkappa_{x\nu} x + B_\nu \sinh \varkappa_{x\nu} x)\, e^{i k_{z\nu} z} \qquad \text{(A5)}$$

and

$$E_z = \frac{i}{\epsilon_o \omega} \frac{\partial H_y}{\partial x}$$

$$= \frac{i}{\epsilon_o \omega} \sum_{-\infty}^{\infty} \varkappa_{x\nu} (A_\nu \sinh \varkappa_{x\nu} x + B_\nu \cosh \varkappa_{x\nu} x)\, e^{i k_{z\nu} z} \qquad \text{(A6)}$$

where $\varkappa_{x\nu} = i\, k_{x\nu}$ and A_ν and B_ν are the excitation coefficients of the partial waves. Using (A1) we may eliminate B_ν to get

$$H_y = \sum_{-\infty}^{\infty} \frac{A_\nu}{\sigma_{o\nu}} \left(\sigma_{o\nu} \cosh \varkappa_{x\nu} x + i \sigma_{s\nu} \sinh \varkappa_{x\nu} x \right) e^{i k_{z\nu} z} \tag{A7}$$

and

$$E_z = \sum_{-\infty}^{\infty} A_\nu \left(i \sigma_{o\nu} \sinh \varkappa_{x\nu} x - \sigma_{s\nu} \cosh \varkappa_{x\nu} x \right) e^{i k_{z\nu} z} \tag{A8}$$

where $\sigma_{o\nu} = \varkappa_{x\nu} / \omega \epsilon_o$. Once the unknown quantity A_ν is determined, all field quantities are uniquely specified.

Each slit of width 'a' and depth 's' of the Millman line acts as a parallel plate transmission line short circuited at $x = -(b + s)$. Accordingly, the field in the mth slit (the zeroeth slit lies at the origin $z = 0$) are given using (A2) and the transmission line equations as

$$E_z(x) = E_{zb} \frac{\sin[k_o (b + s + x)]}{\sin k_o s} e^{i m \psi} \tag{A9}$$

and

$$H_y(x) = i \epsilon_o c E_{zb} \frac{\cos[k_o (b + s + x)]}{\sin k_o s} e^{i m \psi} \tag{A10}$$

We have assumed that the edge effect which will alter E_z at $x = -b$ and introduce a stray component E_x is absent. Also, the field component E_y due to the reaction of the plasma on the circuit has been neglected. Matching E_z from (A8) and (A9) at $x = -b$ gives

$$\sum_{-\infty}^{\infty} A_\nu \left(-i \sigma_{o\nu} \sinh \varkappa_{x\nu} b - \sigma_{s\nu} \cosh \varkappa_{x\nu} b \right) e^{i k_{z\nu} z}$$

$$= \begin{cases} E_{zb} e^{i m \psi} & , \text{ if } z \text{ lies within a slit} \\ 0 & , \text{ if } z \text{ lies outside a slit} \end{cases} \tag{A11}$$

Fourier transforming both sides of (A11) in the interval $z = mL - L/2$ to $z = mL + L/2$ gives

$$-A_\nu(i\sigma_{o\nu}\sinh \varkappa_{x\nu} b + \sigma_{s\nu}\cosh \varkappa_{x\nu} b)\ \frac{k_{z\nu}\, a/2}{\sin(k_{z\nu} a/2)} = \frac{a}{L} E_{zb} \qquad \text{(A12)}$$

which finally determines A_ν. Using (A7), (A8) and (A12), the field components at $x = -b$ may be written as

$$E_z = \frac{a}{L} E_{zb} \sum_{-\infty}^{\infty} \frac{\sin(k_{z\nu} a/2)}{k_{z\nu} a/2}\, e^{i k_{z\nu} z} \qquad \text{(A13)}$$

and

$$H_y = \frac{a}{L} E_{zb} \sum_{-\infty}^{\infty} \frac{i}{\sigma_{o\nu}}\ \frac{\sin(k_{z\nu} a/2)}{k_{z\nu} a/2}\ \frac{\sigma_{o\nu} - i\sigma_{s\nu}\tanh \varkappa_{x\nu} b}{\sigma_{o\nu}\tanh \varkappa_{x\nu} b - i\sigma_{s\nu}}\, e^{i k_{z\nu} z} \qquad \text{(A14)}$$

As an example, let us calculate E_z and H_y for the representative case $n_{zo} = 1.5$, $\omega_{pe}/\omega_{ce} = 0.57$ discussed in Sec. IV. Choice of $\psi_o = \pi/2$ or $L/\lambda = 1/4$ results in $n_{zo} = \lambda_o/\lambda = 1.5$. Assuming $b/L = 1$ and $a/L = 1/2$, the normalized computed $|E_{z\nu}|$ and $|H_{y\nu}|$ are given in Table 2. Note that except for the fundamental harmonic $\nu = 0$, $\varkappa_{x\nu} b \gg 1$, $\tanh \varkappa_{x\nu} b \to 1$ so that the factor containing tanh in (A14) tends also to unity and it is not necessary to know $\sigma_{s\nu}$ for $\nu \neq 0$ for the determination of H_y in (A14).

In order to complete the description of the slow-wave structure, it remains to determine the quantity 's' (Fig. 21). This is accomplished through the dispersion relation. Matching H_y in (A7) and (A10) at $x = -b$ gives

$$\frac{1}{a}\int_{mL-\frac{a}{2}}^{mL+\frac{a}{2}} \sum_{-\infty}^{\infty} \frac{A_\nu}{\sigma_{o\nu}}(\sigma_{o\nu}\cosh \varkappa_{x\nu} b - i\sigma_{s\nu}\sinh \varkappa_{x\nu} b)\, e^{i k_{z\nu} z}\, dz$$

$$= i\epsilon_o c\, E_{zb} \cot(k_o s)\, e^{im\psi}$$

or

$$\sum_{-\infty}^{\infty} \frac{A_\nu}{\sigma_{o\nu}}(\sigma_{o\nu}\cosh \varkappa_{x\nu} b - i\sigma_{s\nu}\sinh \varkappa_{x\nu} b)\ \frac{\sin(k_{z\nu} a/2)}{k_{z\nu} a/2} \qquad \text{(A15)}$$

$$= i\epsilon_o c\, E_{zb} \cot(k_o s)$$

Dividing (A15) by (A12) gives the desired dispersion relation

$$\sum_{-\infty}^{\infty} \frac{\sigma_o}{\sigma_{o\nu}} \frac{\sigma_{o\nu} - i\sigma_{s\nu} \tanh \varkappa_{x\nu} b}{\sigma_{o\nu} \tanh \varkappa_{x\nu} b - i\sigma_{s\nu}} \left[\frac{\sin(k_{z\nu} a/2)}{k_{z\nu} a/2} \right]^2 = \frac{L}{a} \cot(k_o s) \quad \text{(A16)}$$

where $\sigma_o = (\mu_o/\epsilon_o)^{1/2}$ is the impedance of free space. From (A16), the value of 's' for the example considered above is given by

$$\frac{s}{\lambda_o} = 0.165 \qquad \text{or} \qquad \frac{s}{L} \approx 1.$$

From dispersion relation (A16) we can also calcualte the group velocity

$$v_{gz} = L \frac{\partial \omega}{\partial \psi_o} = 0.64\, c.$$

LIST OF TABLE CAPTIONS

Table I. The normalized plasma parameters used for the five curves in Figs. 6 and 7. The representative case in Sec. IV employs the parameters of Case 3 of this table. Note that ω/ω_{ci} is uniquely related to ω_{pe}/ω_{ce}.

Table II. Normalized values of E_z and H_y at the edge ($x = -b$) of the Millman line for various harmonics of the slow-wave field. The value of $\sigma_{s\nu}$ for $n_z = 1.5$ is obtained from curve 3 of Fig. 6. As pointed out in the text, it is not necessary to know $\sigma_{s\nu}$ for other values of n_z.

LIST OF FIGURE CAPTIONS

Fig. 1 The plasma model used for the case of TE excitation. The exciting current J_s at $x = -b$ is assumed to be a sheet of zero thickness.

Fig. 2 The critical value n_{zo} beyond which accessibility occurs is shown as a function of ω/ω_{ci} (or ω_{pe}/ω_{ce}) using the criteria developed by Stix, Parker and Golant. The solid curve shows the exactly computed results.

Fig. 3 The propagation constant k_x vs x for $\omega/\omega_{ci} = 10$ for both the slow and the fast waves for three different values of n_z. The unprimed and primed pairs are for the cases $\langle \nu_{ei} \rangle / \omega = 0$ and $\langle \nu_{ei} \rangle / \omega \sim 10^{-2}$, respectively.

Fig. 4 The propagation constant k_x vs x for $\omega/\omega_{ci} = 30$ for both the slow and the fast waves for three different values of n_z. The unprimed and primed pairs are for the cases $\langle \nu_{ei} \rangle / \omega = 0$ and $\langle \nu_{ei} \rangle / \omega \sim 10^{-2}$, respectively.

Fig. 5 The propagation constant k_x vs x for $\omega/\omega_{ci} = 50$ for both the slow and the fast waves for three different values of n_z. The unprimed and primed pairs are for the cases $\langle \nu_{ei} \rangle / \omega = 0$ and $\langle \nu_{ei} \rangle / \omega \sim 10^{-2}$, respectively.

Fig. 6 The x-component P_x of the Poynting vector as a function of n_z for five different values of ω_{pe}/ω_{ce} (given in Table I) for TM excitation are shown by

the solid curves (a). The dashed lines in (a) show the power coupled when the plasma is substituted by stainless steel. The real and imaginary parts of the surface impedance $\sigma_s = - E_z/H_y$ are shown in (b).

Fig. 7 The x-component P_x of the Poynting vector as a function of n_z for five different values of ω_{pe}/ω_{ce} (given in Table I) for TE excitation are shown by the solid curves (a). The dashed lines in (a) show the power coupled when the plasma is substituted by stainless steel. The real and imaginary parts of the surface impedance $\sigma_s = E_y/H_z$ are shown in (b).

Fig. 8 The x-component of the electric field amplitude of the fast and the slow waves, both for the TM and TE polarizations.

Fig. 9 The phases of the x-component of the electric field of the fast and the slow waves, both for the TM and TE polarizations. The vertical scale is to be read with the positive sign for the fast wave and the negative sign for the slow wave.

Fig. 10 The amplitude and the phase of the combined electric field $E_x + E_y$ at $z = 0$ due to the fast and slow waves for TM excitation.

Fig. 11 The amplitude and the phase of the combined electric field $E_x + E_y$ at $z = 0$ due to the fast and slow waves for TE excitation.

Fig. 12 The electric field configuration in the x-z plane for TM excitation.

Fig. 13 The magnetic field configuration in the x-z plane for TE excitation.

Fig. 14 The Poynting vector components P_x, P_y and P_z as a function of x for the case of TM excitation.

Fig. 15 The polar projection of Poynting vector components P_y and P_z as a function of x (values marked along the curve) for TM excitation.

Fig. 16 The Poynting vector components P_x, P_y and P_z as a function of x for the case of TE excitation.

Fig. 17 The polar projection of Poynting vector components P_y and P_z as a function of x (values marked along the curve) for TE excitation.

Fig. 18 Group and energy velocity components both for TM and TE excitation.

Fig. 19 Three dimensional representation of pulse propagation for TM excitation, assuming that the pulse travels with the energy velocity.

Fig. 20 Three dimensional representation of pulse propagation for TE excitation, assuming that the pulse travels with the energy velocity.

Fig. 21 Approximation of magnetic current excitation with a Millman line.

Table 1

Curve in Figs.6 & 7	ω/ω_{ci}	ω_{pe}/ω_{ce}	T ^{o}K	$<\nu_{ei}>/\omega$
1	10	0.17	3.0×10^{4}	10^{-2}
2	20	0.35	5.1×10^{4}	10^{-2}
3	30	0.57	7.4×10^{4}	10^{-2}
4	40	0.88	1.1×10^{5}	10^{-2}
5	50	1.46	1.9×10^{5}	10^{-2}

Table 2

ν	$n_{z\nu}$	$\varkappa_{x\nu} b$	$\tanh \varkappa_{x\nu} b$	$\sigma_{s\nu}$	$E_{z\nu}/E_{zo}$	$H_{y\nu}/H_{yo}$
-2	-10.5	10.90	$\sim 1.$		0.14	0.01
-1	- 4.5	4.60	$\sim 1.$		0.81	0.17
0	1.5	1.17	0.82	10 - i 100	1.	1.
1	7.5	7.80	$\sim 1.$		0.48	0.06
2	13.5	14.10	$\sim 1.$		0.11	0.01

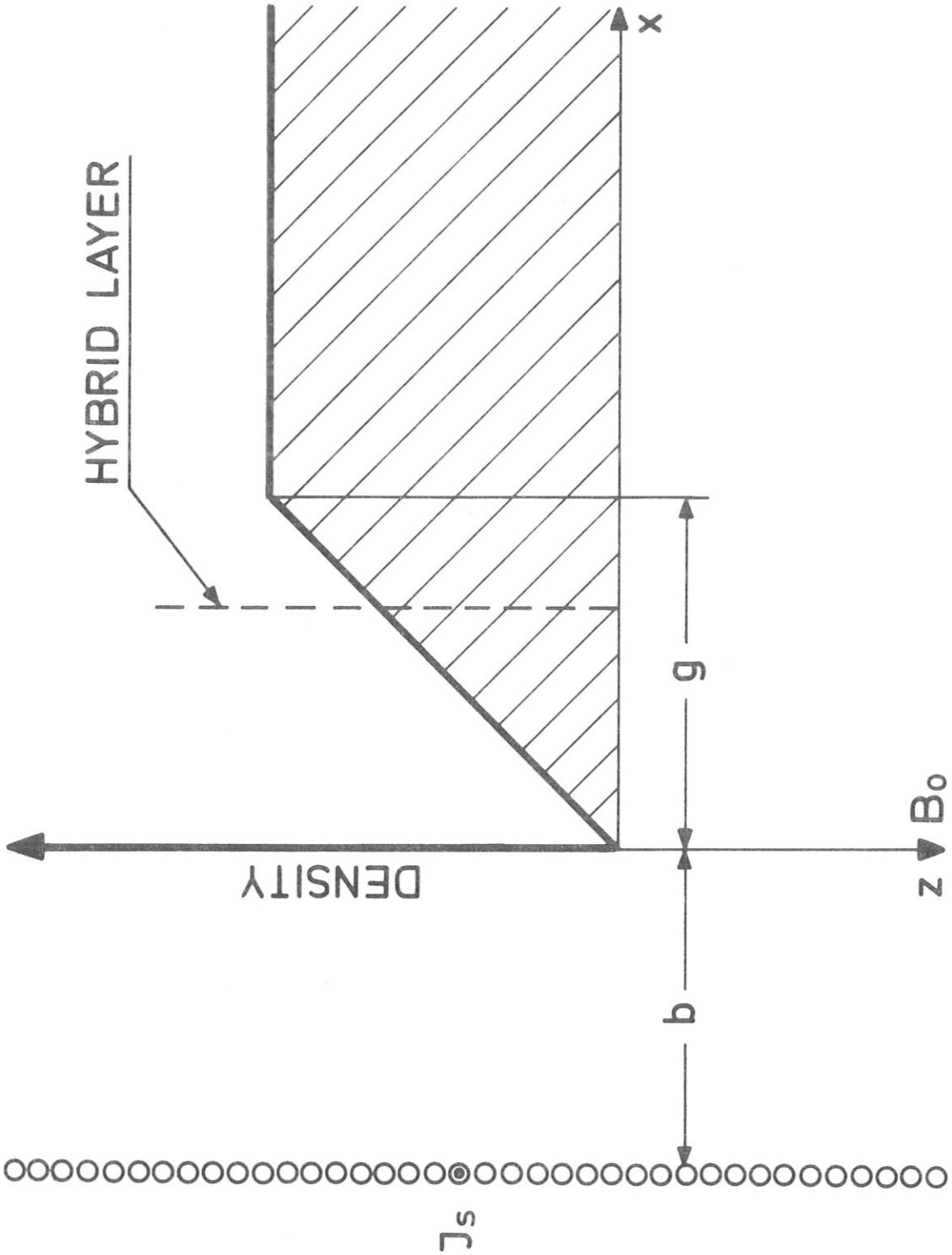

Fig. 1

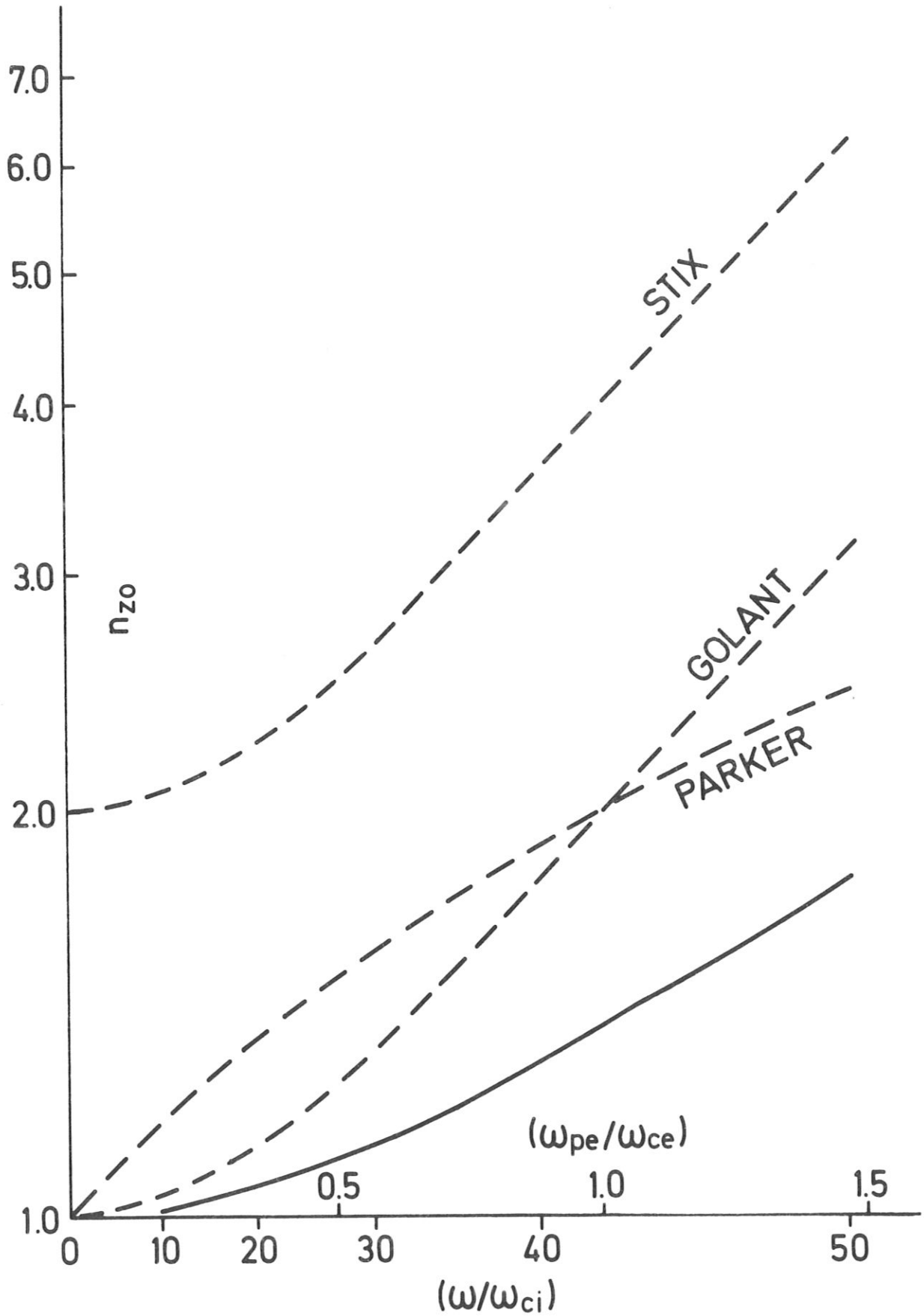
7.0
6.0
5.0
4.0
3.0
2.0
1.0
n_{zo}
STIX
GOLANT
PARKER
$(\omega_{pe}/\omega_{ce})$
0.5
1.0
1.5
0
10
20
30
40
50
(ω/ω_{ci})

Fig. 2

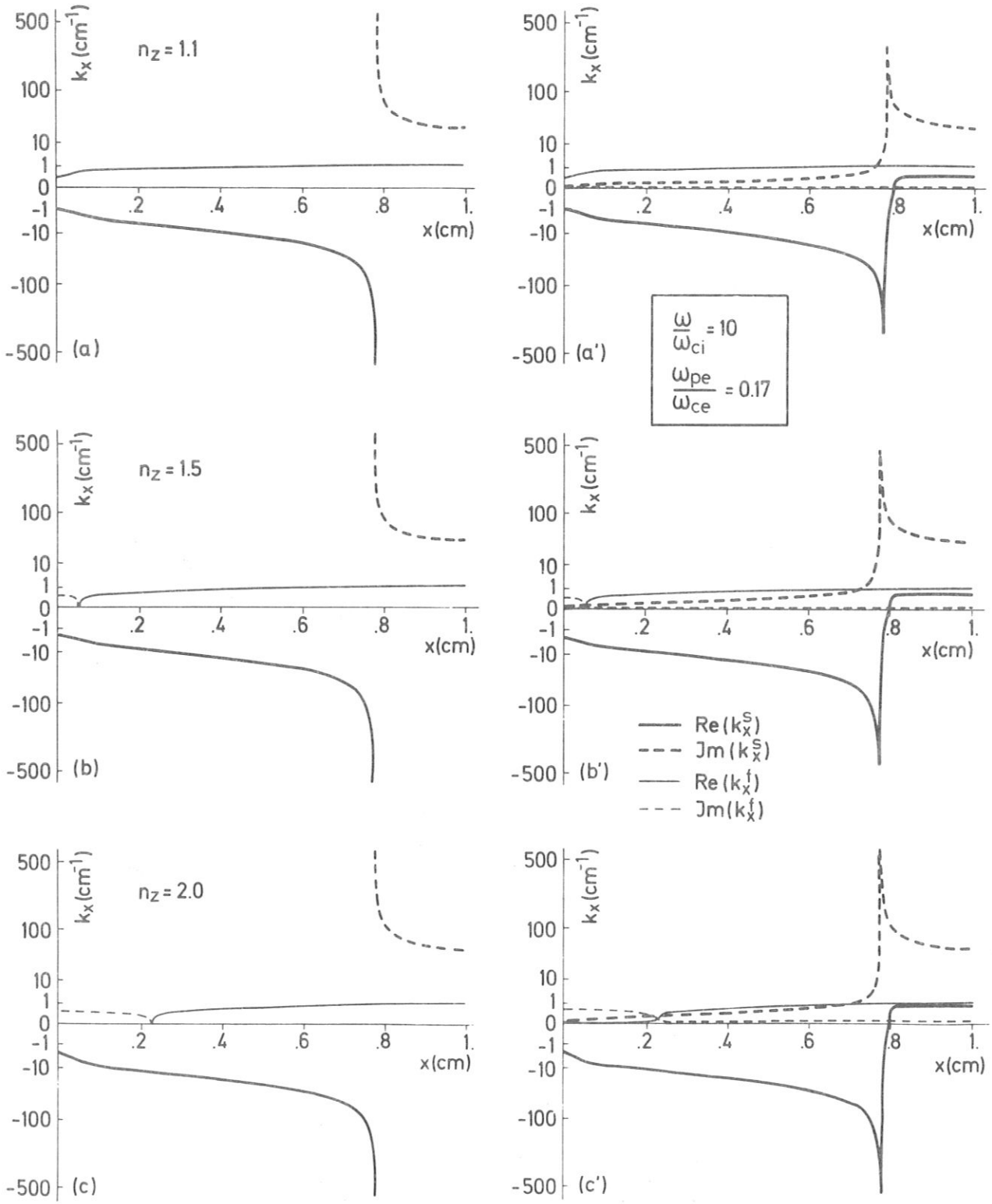
$n_z = 1.1$
$n_z = 1.5$
$n_z = 2.0$
$k_x\,(cm^{-1})$
x(cm)
(a)
(a')
(b)
(b')
(c)
(c')
$\frac{\omega}{\omega_{ci}} = 10$
$\frac{\omega_{pe}}{\omega_{ce}} = 0.17$
$Re(k_x^s)$
$Jm(k_x^s)$
$Re(k_x^f)$
$Jm(k_x^f)$

Fig. 3

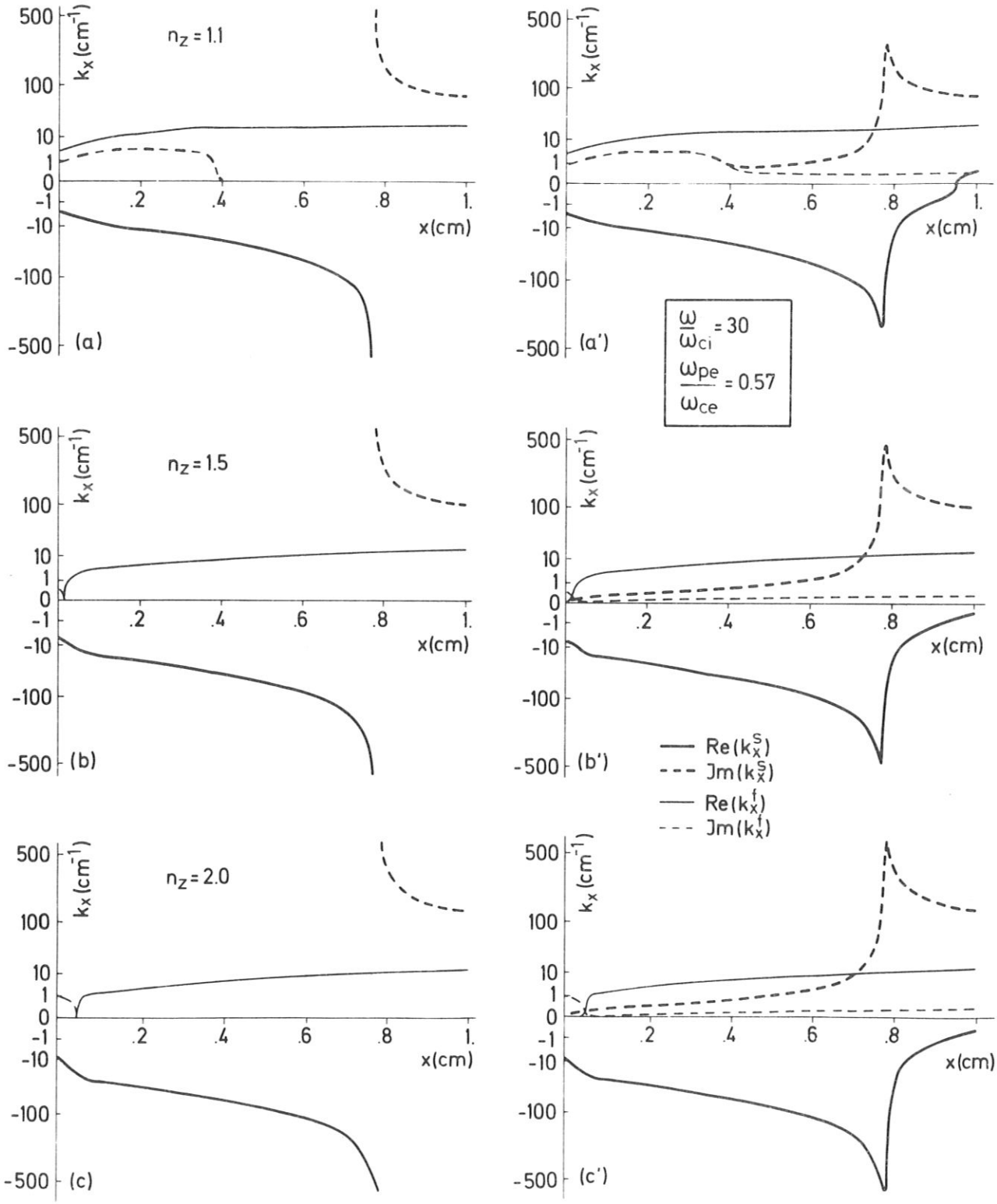
$n_z = 1.1$
$n_z = 1.5$
$n_z = 2.0$
$k_x (cm^{-1})$
x(cm)
(a)
(b)
(c)
(a')
(b')
(c')
$\frac{\omega}{\omega_{ci}} = 30$
$\frac{\omega_{pe}}{\omega_{ce}} = 0.57$
$Re(k_x^s)$
$Im(k_x^s)$
$Re(k_x^f)$
$Im(k_x^f)$

Fig. 4

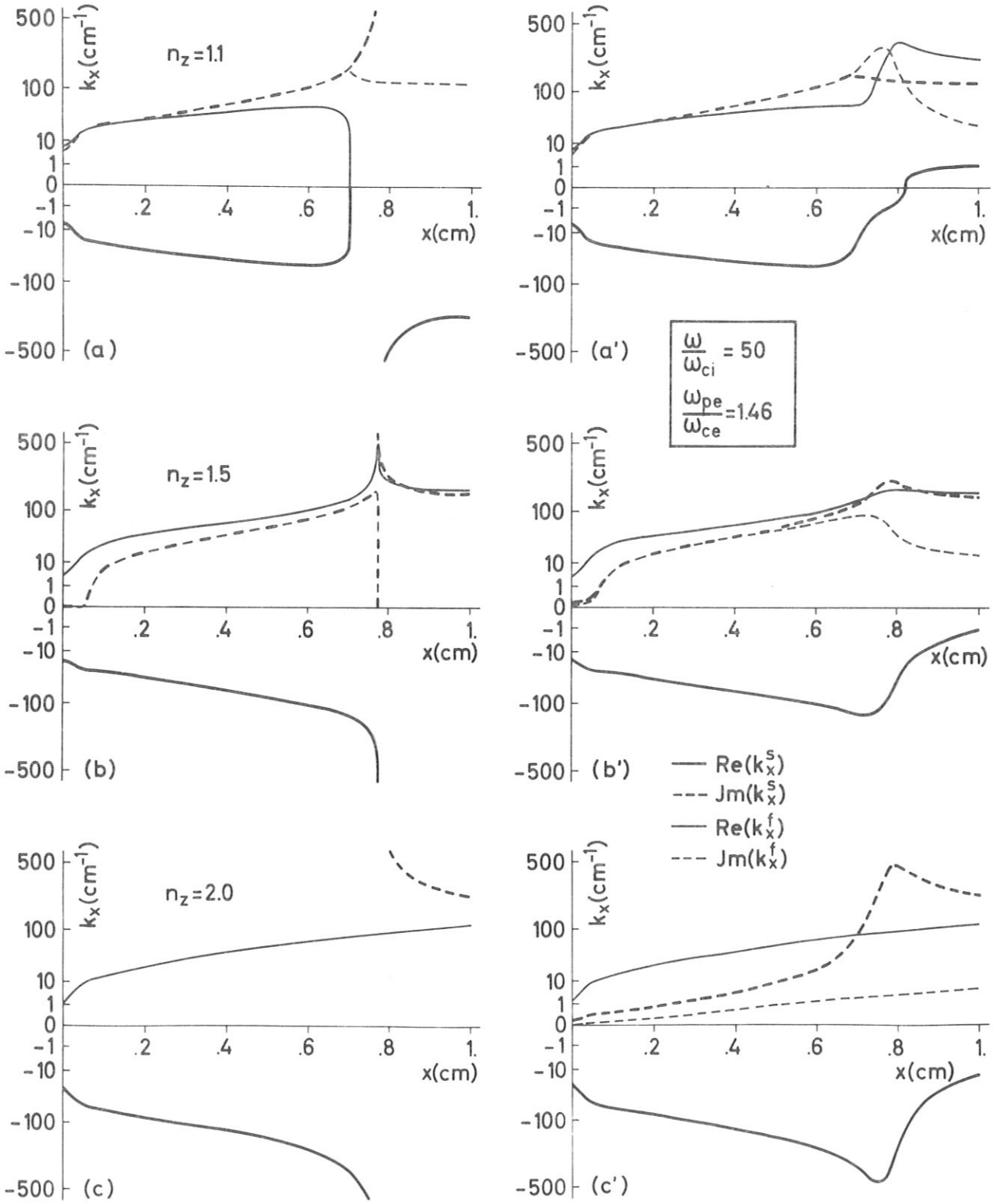
n_z=1.1
k_x(cm^{-1})
x(cm)
(a)
(a')
$\frac{\omega}{\omega_{ci}}$ = 50
$\frac{\omega_{pe}}{\omega_{ce}}$=1.46
n_z=1.5
(b)
(b')
Re(k_x^s)
Jm(k_x^s)
Re(k_x^f)
Jm(k_x^f)
n_z=2.0
(c)
(c')

Fig. 5

Fig. 6

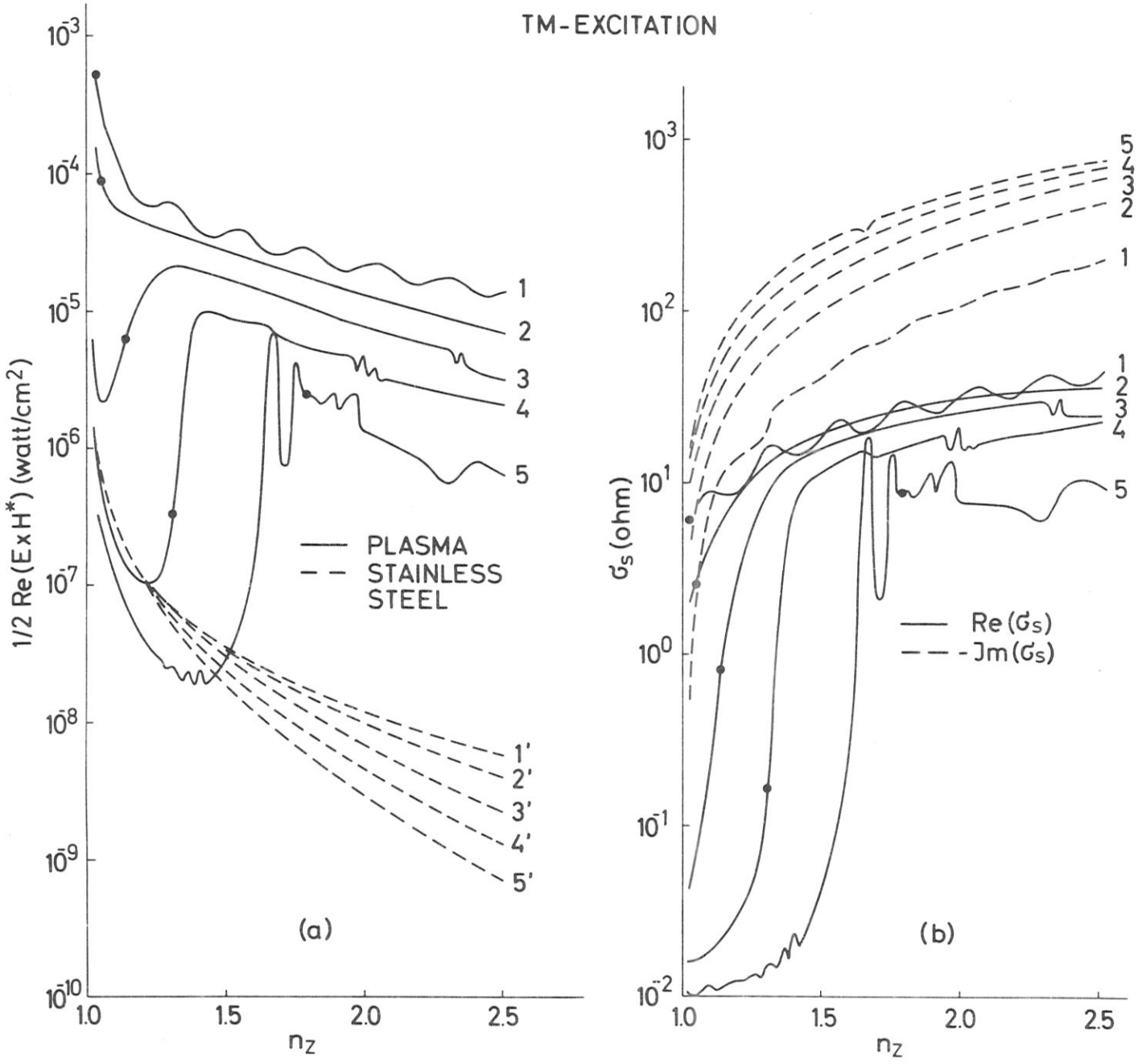
TM-EXCITATION
1/2 Re(E x H*) (watt/cm²)
PLASMA
STAINLESS STEEL
(a)
n_z
σ_s (ohm)
Re (σ_s)
- Jm (σ_s)
(b)
n_z

Fig. 7

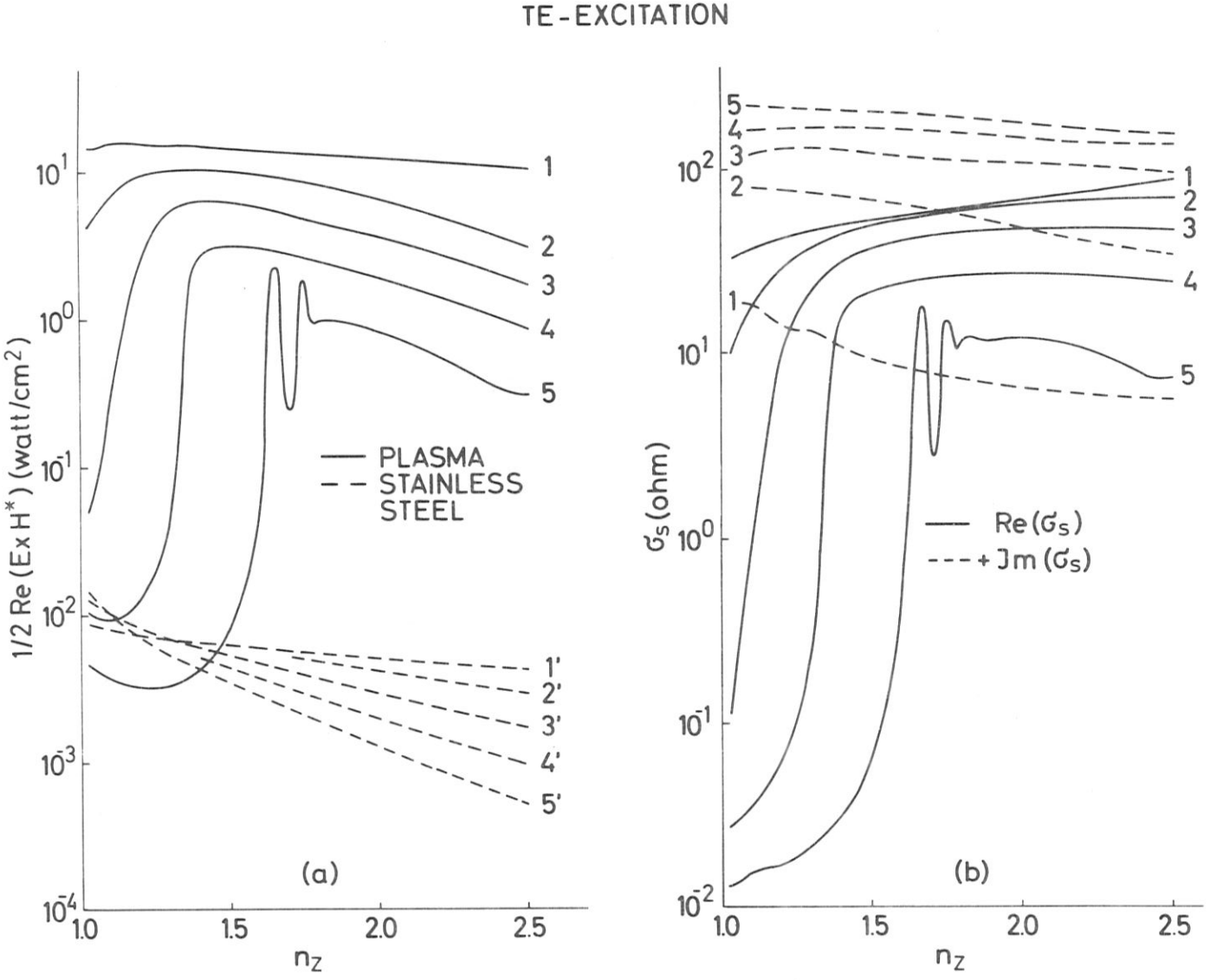
TE-EXCITATION
1/2 Re (E x H*) (watt/cm²)
PLASMA
STAINLESS STEEL
(a)
nz
σs (ohm)
Re (σs)
+ Jm (σs)
(b)
nz

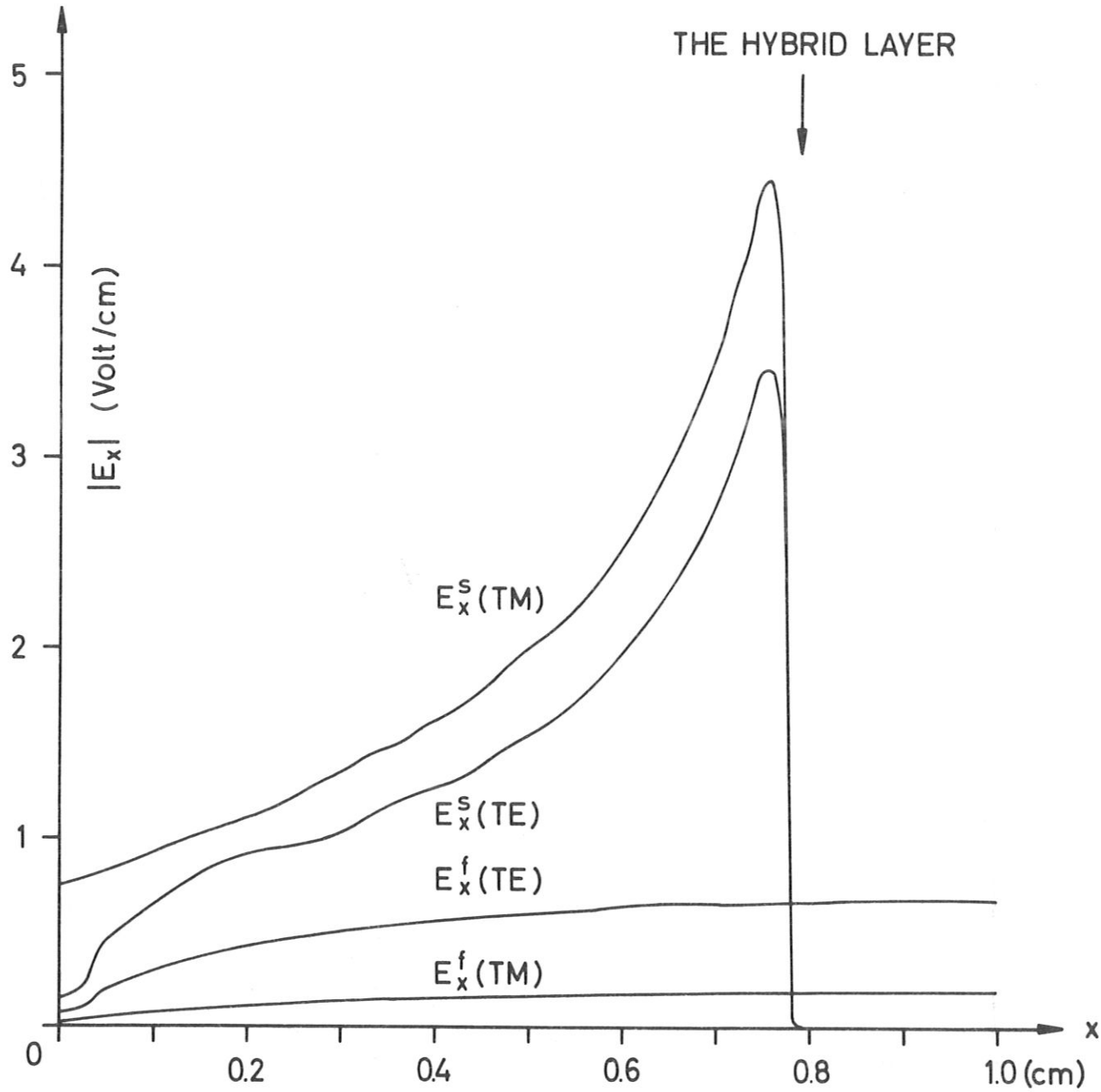
THE HYBRID LAYER
5
4
3
2
1
0
|Ex| (Volt/cm)
E_x^s(TM)
E_x^s(TE)
E_x^f(TE)
E_x^f(TM)
x
0.2
0.4
0.6
0.8
1.0 (cm)

Fig. 8

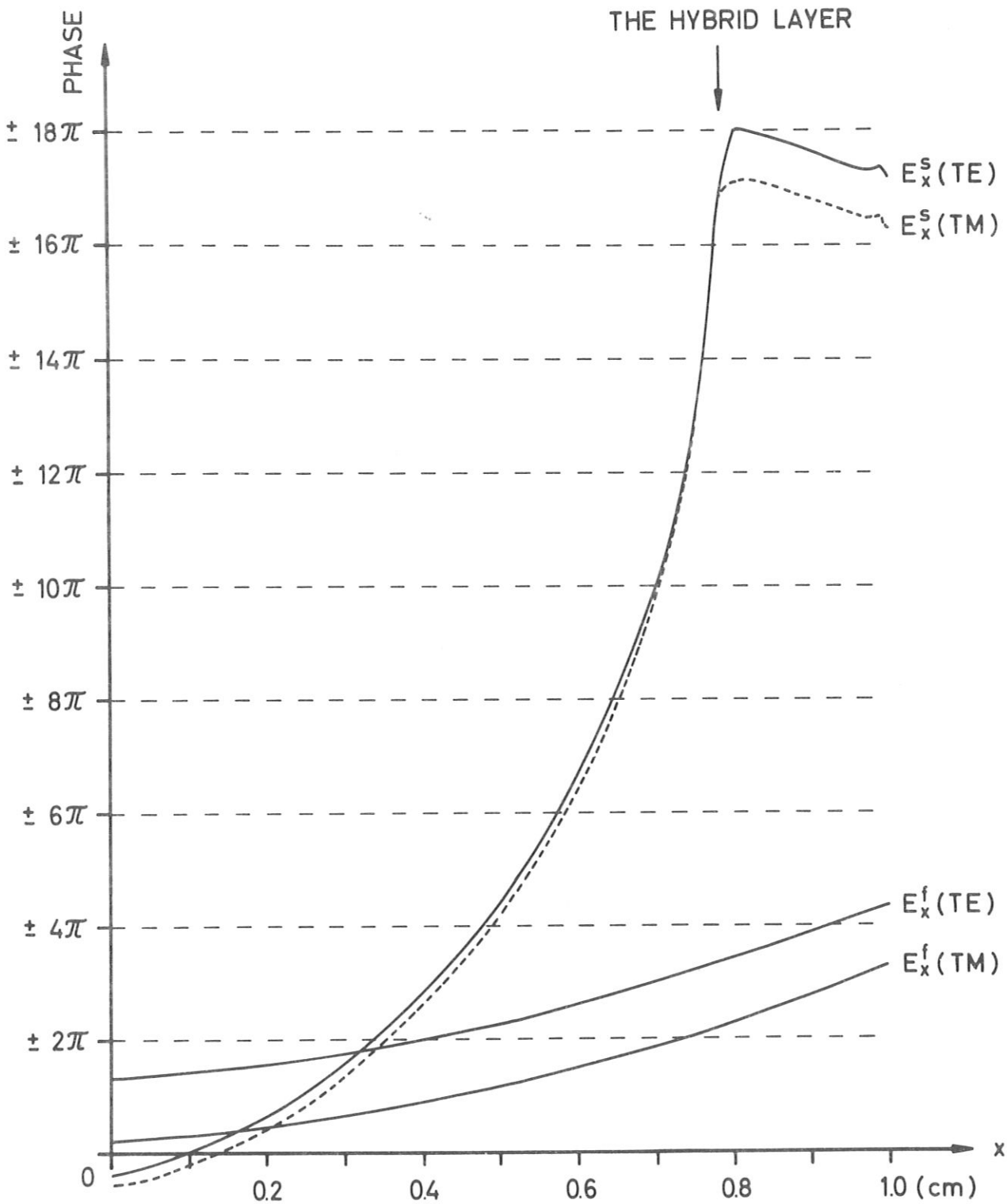
THE HYBRID LAYER
PHASE
± 18π
± 16π
± 14π
± 12π
± 10π
± 8π
± 6π
± 4π
± 2π
0
0.2
0.4
0.6
0.8
1.0 (cm)
x
E_x^s(TE)
E_x^s(TM)
E_x^f(TE)
E_x^f(TM)

Fig. 9

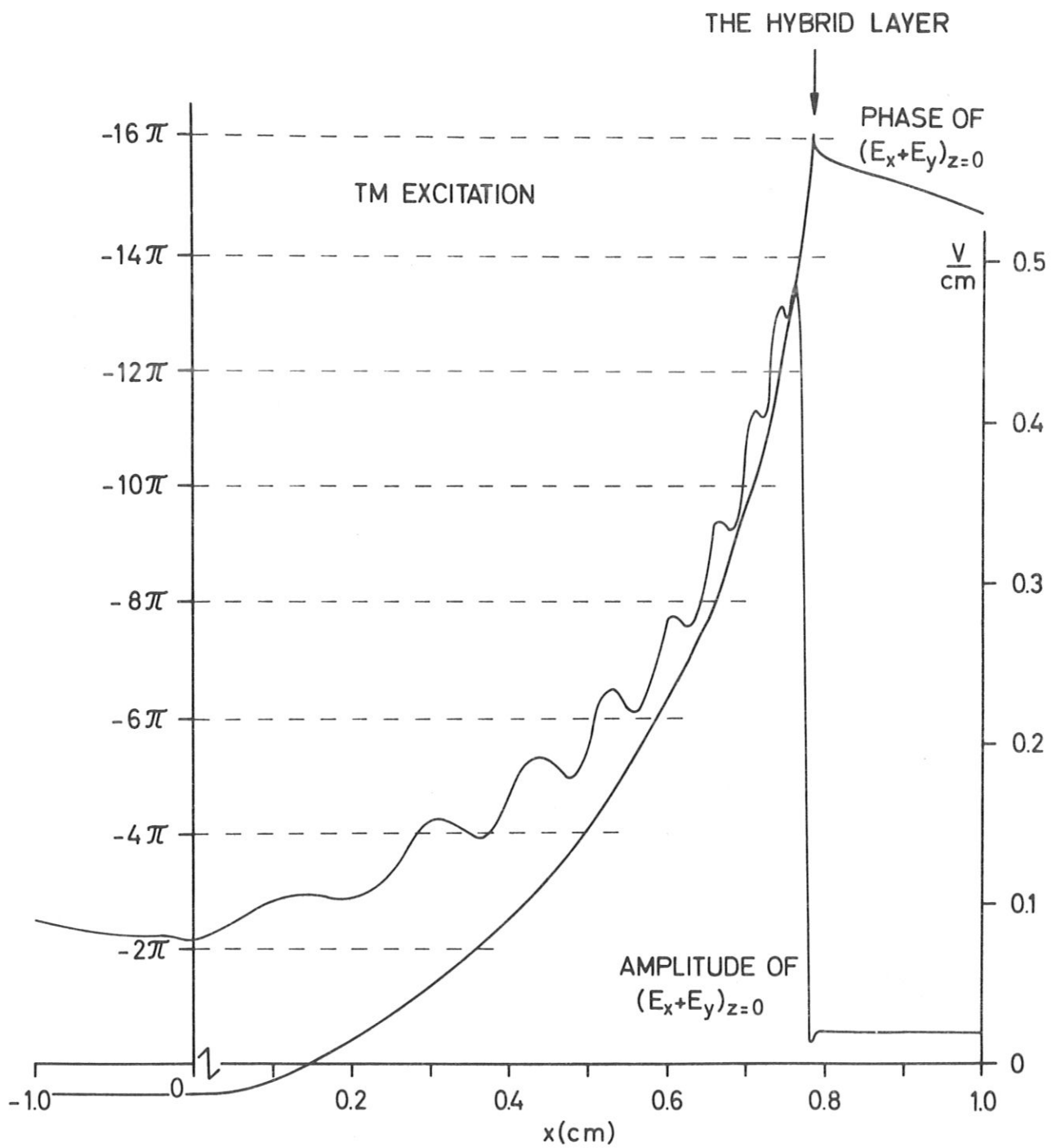
THE HYBRID LAYER
PHASE OF
$(E_x+E_y)_{z=0}$
TM EXCITATION
-16π
-14π
-12π
-10π
-8π
-6π
-4π
-2π
V/cm
0.5
0.4
0.3
0.2
0.1
0
AMPLITUDE OF
$(E_x+E_y)_{z=0}$
-1.0
0
0.2
0.4
0.6
0.8
1.0
x(cm)

Fig. 10

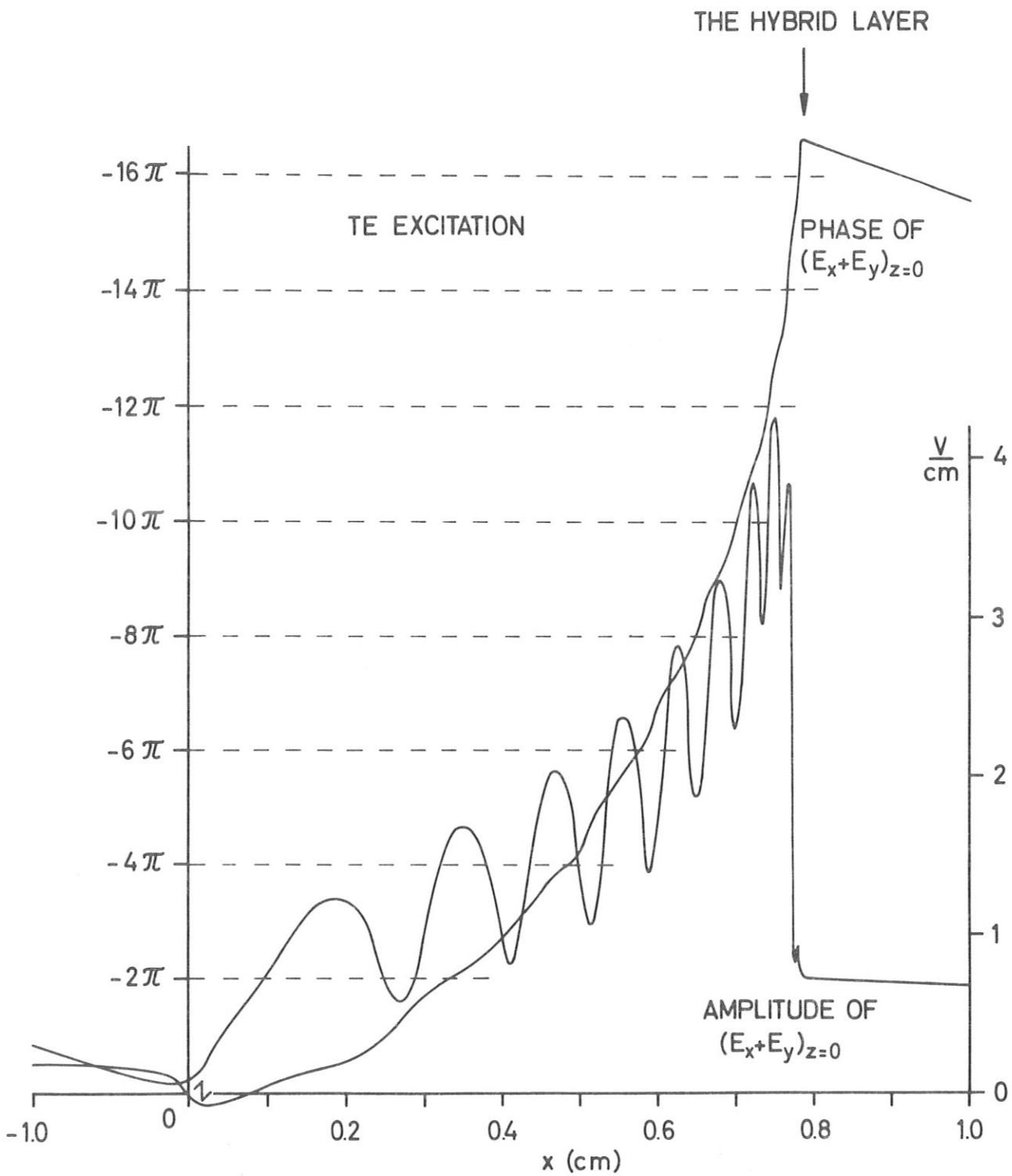
THE HYBRID LAYER
TE EXCITATION
PHASE OF
$(E_x+E_y)_{z=0}$
AMPLITUDE OF
$(E_x+E_y)_{z=0}$
-16π
-14π
-12π
-10π
-8π
-6π
-4π
-2π
$\frac{V}{cm}$
4
3
2
1
0
-1.0
0
0.2
0.4
0.6
0.8
1.0
x (cm)

Fig. 11

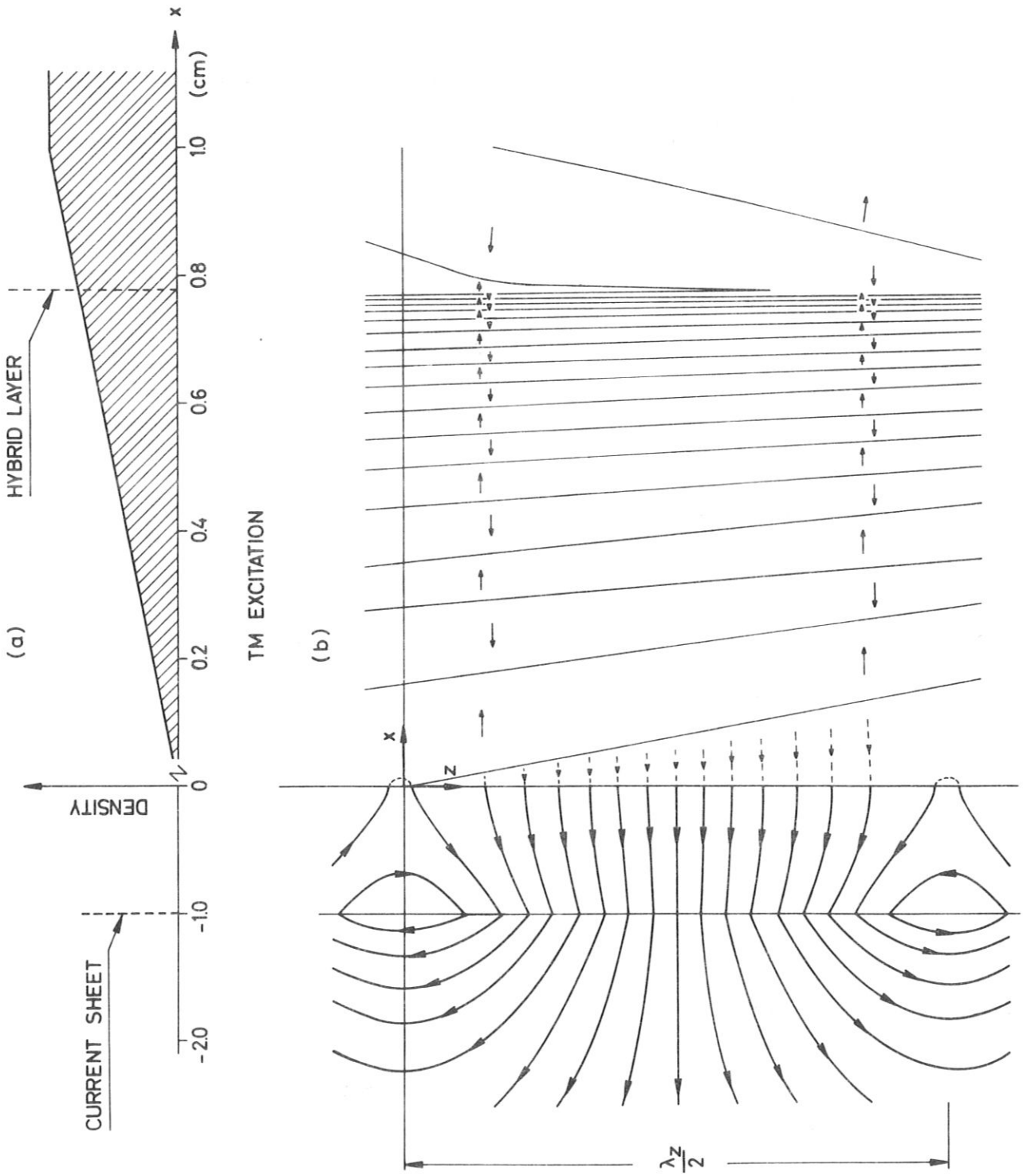
x
(cm)
1.0
0.8
0.6
0.4
0.2
0
-1.0
-2.0
HYBRID LAYER
CURRENT SHEET
DENSITY
(a)
TM EXCITATION
(b)
x
z
$\frac{\lambda z}{2}$

Fig. 12

(a)

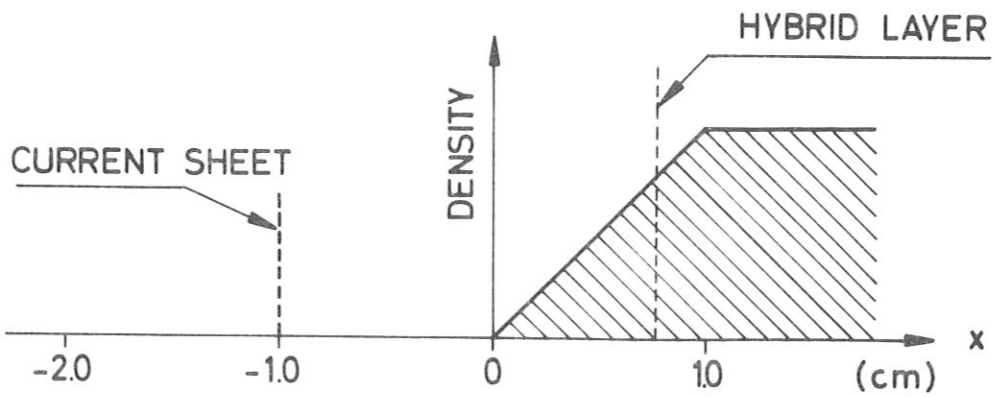

TE EXCITATION

(b)

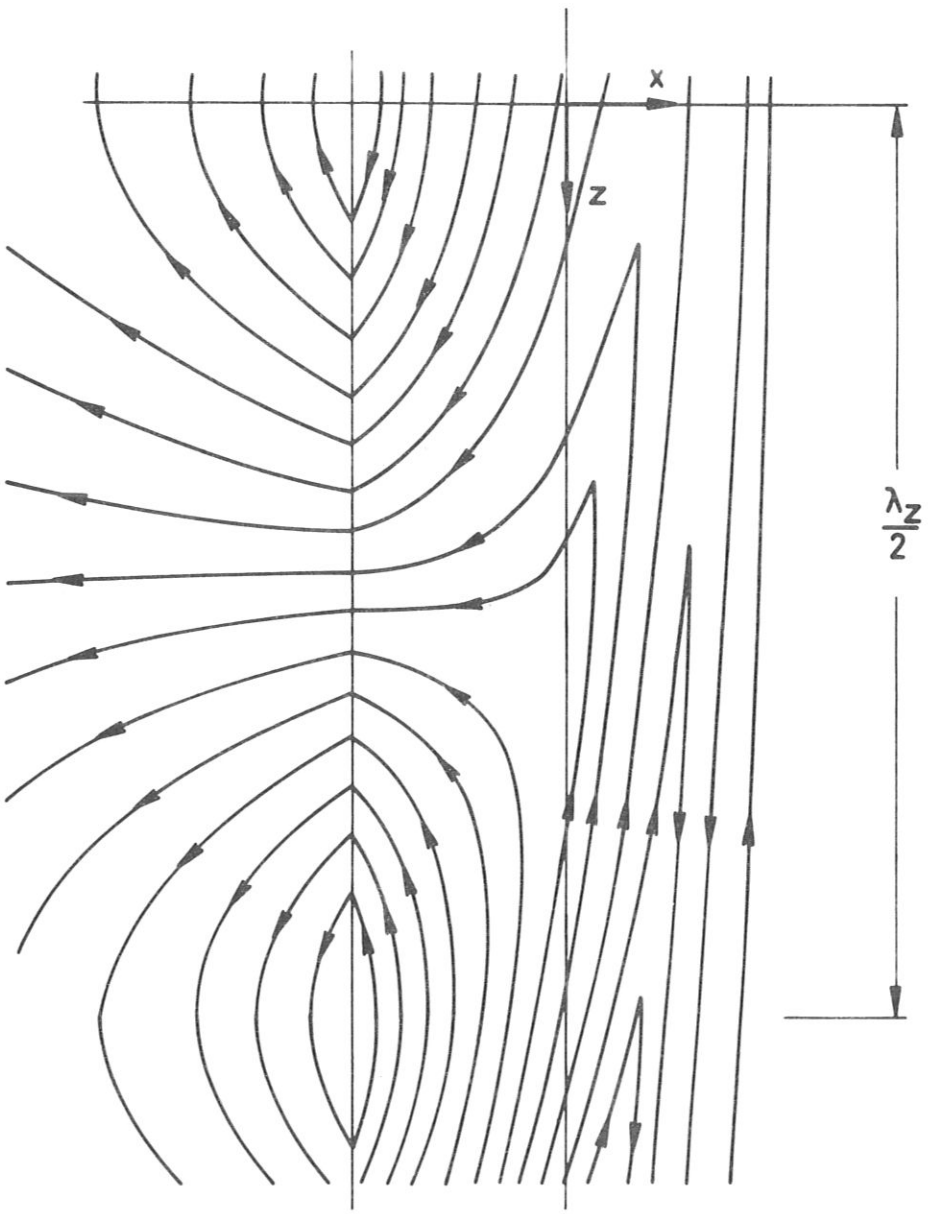

Fig. 13

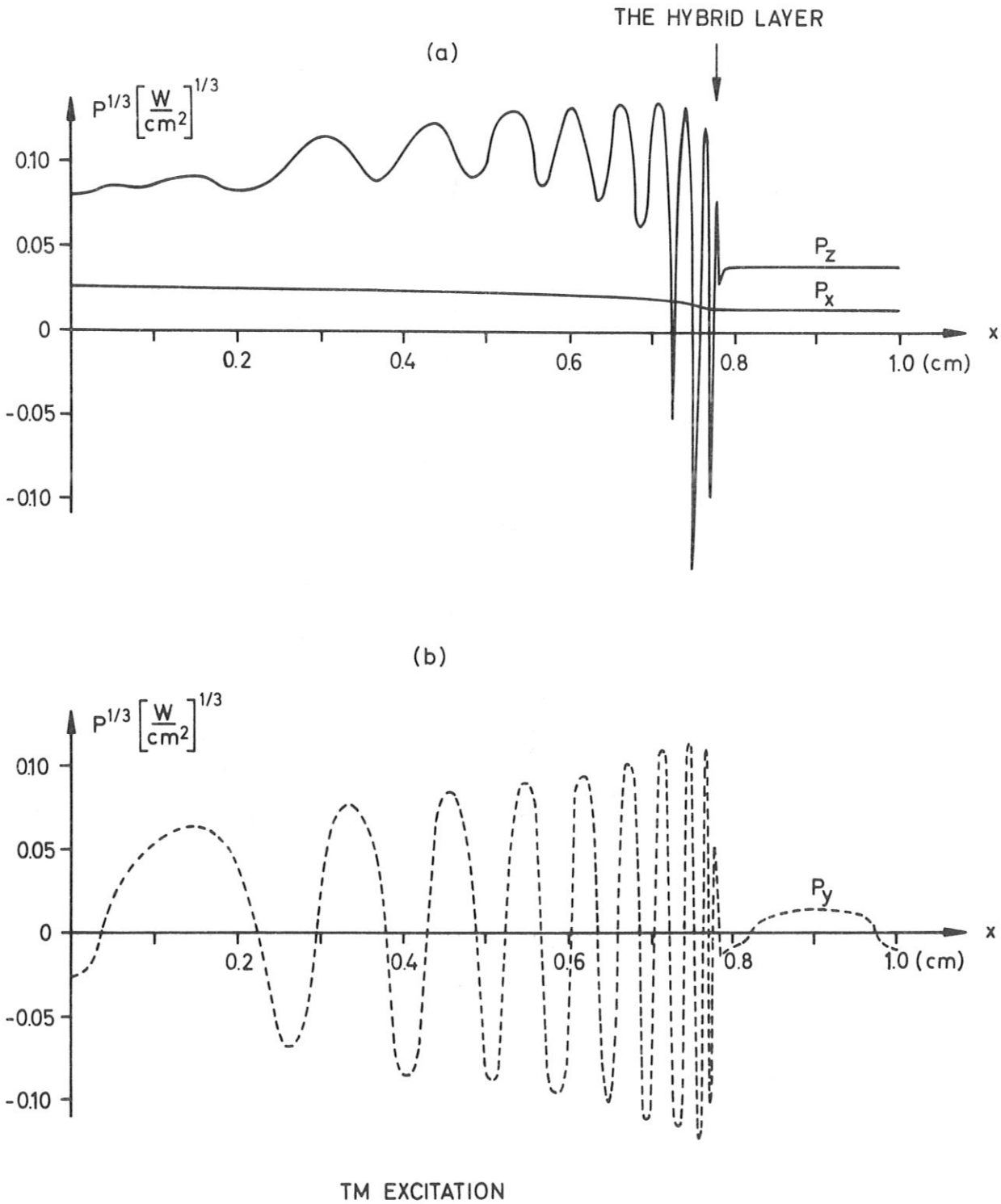
THE HYBRID LAYER
(a)
$P^{1/3}\left[\frac{W}{cm^2}\right]^{1/3}$
0.10
0.05
0
-0.05
-0.10
P_z
P_x
x
0.2
0.4
0.6
0.8
1.0 (cm)
(b)
$P^{1/3}\left[\frac{W}{cm^2}\right]^{1/3}$
0.10
0.05
0
-0.05
-0.10
P_y
x
0.2
0.4
0.6
0.8
1.0 (cm)
TM EXCITATION

Fig. 14

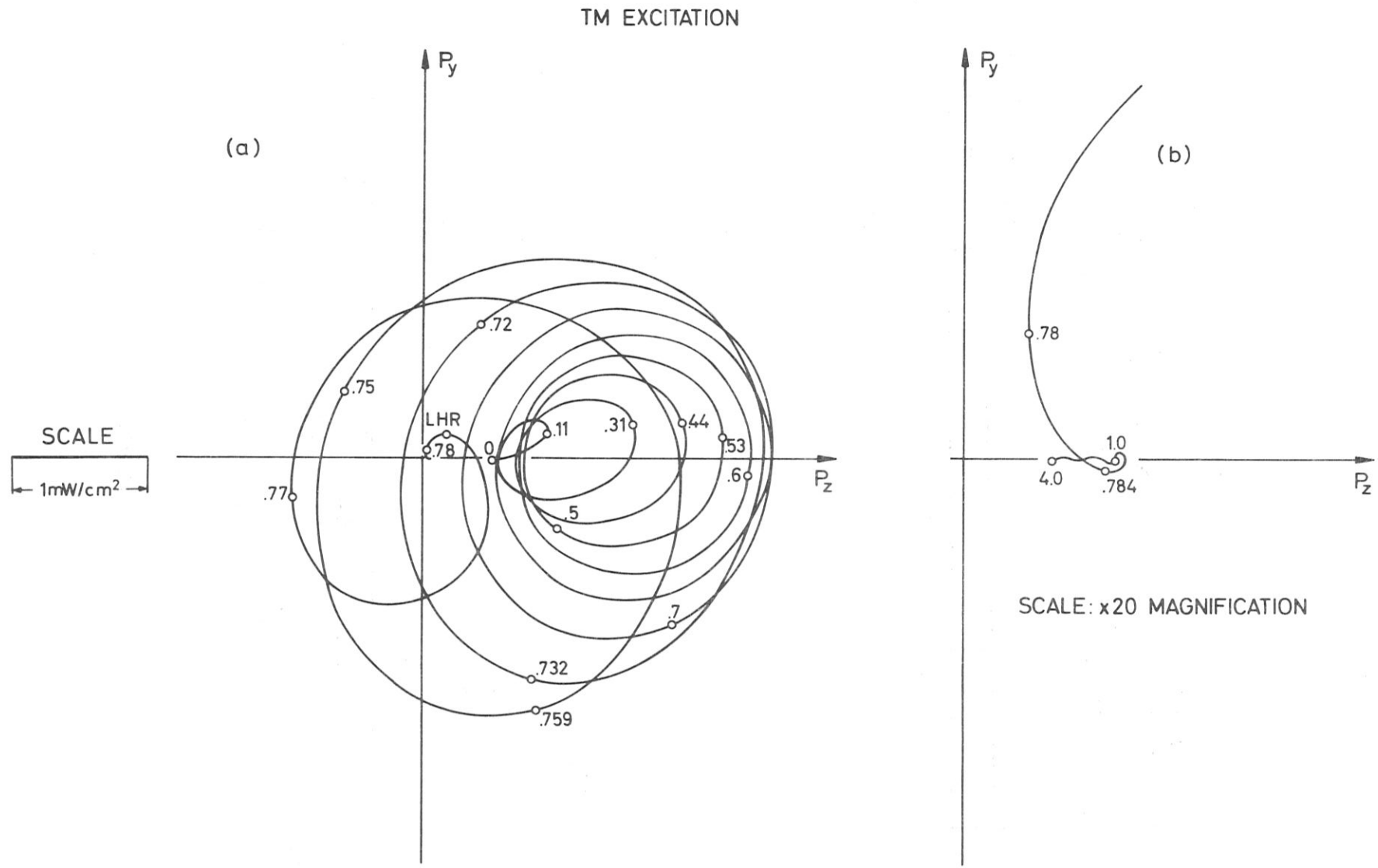
TM EXCITATION
(a)
P_y
P_z
SCALE
1mW/cm²
.72
.75
LHR
.78
0
.11
.31
.44
.53
.6
.77
.5
.7
.732
.759
(b)
P_y
P_z
.78
1.0
4.0
.784
SCALE: x20 MAGNIFICATION

Fig. 15

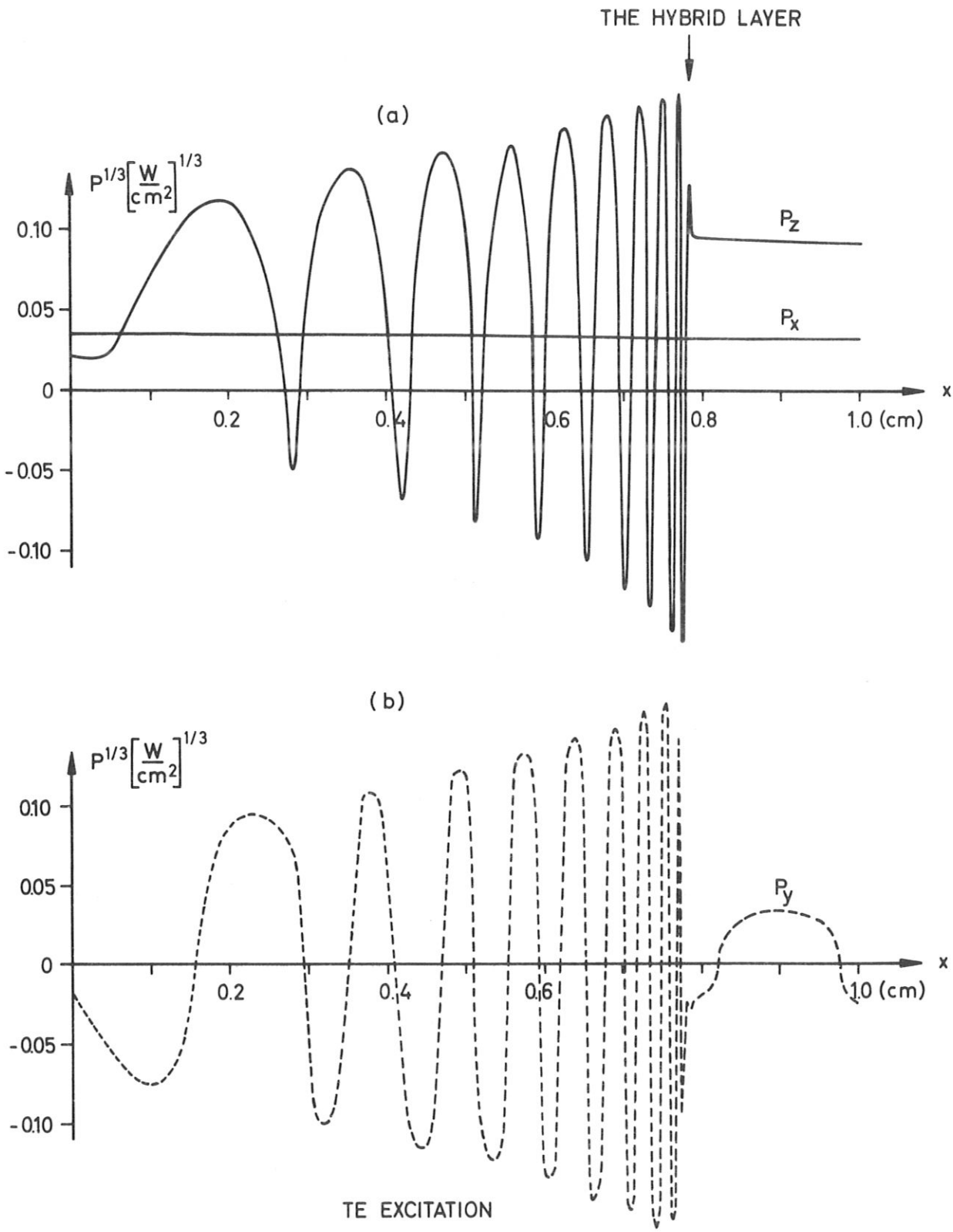
THE HYBRID LAYER
(a)
$P^{1/3}\left[\frac{W}{cm^2}\right]^{1/3}$
0.10
0.05
0
-0.05
-0.10
0.2
0.4
0.6
0.8
1.0 (cm)
x
P_z
P_x
(b)
$P^{1/3}\left[\frac{W}{cm^2}\right]^{1/3}$
0.10
0.05
0
-0.05
-0.10
0.2
0.4
0.6
1.0 (cm)
x
P_y
TE EXCITATION

Fig. 16

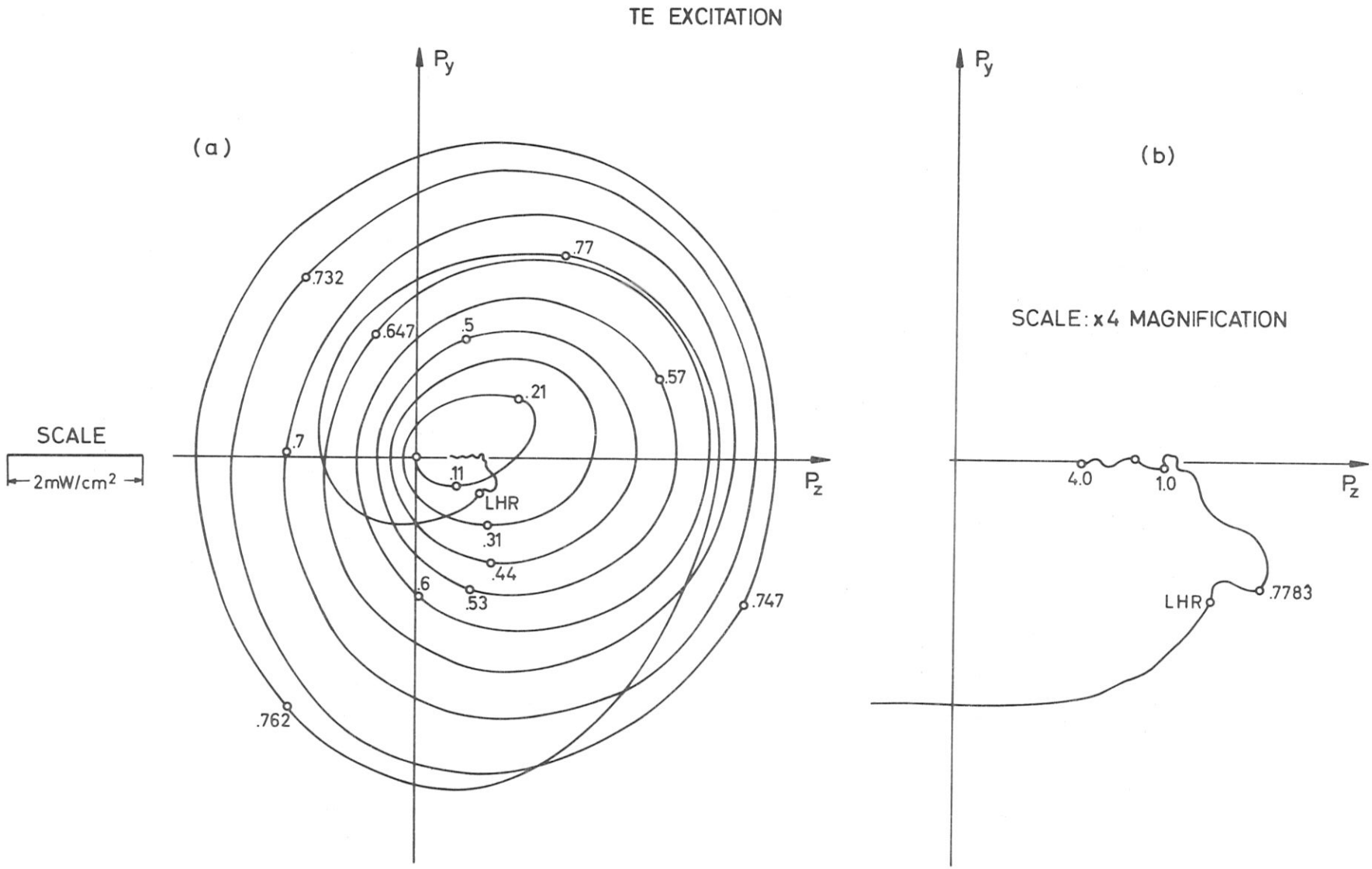
TE EXCITATION
(a)
(b)
P_y
P_z
SCALE
2mW/cm²
.732
.77
.647
.5
.57
.21
.7
.11
LHR
.31
.44
.6
.53
.747
.762
SCALE: x4 MAGNIFICATION
4.0
1.0
LHR
.7783

Fig. 17

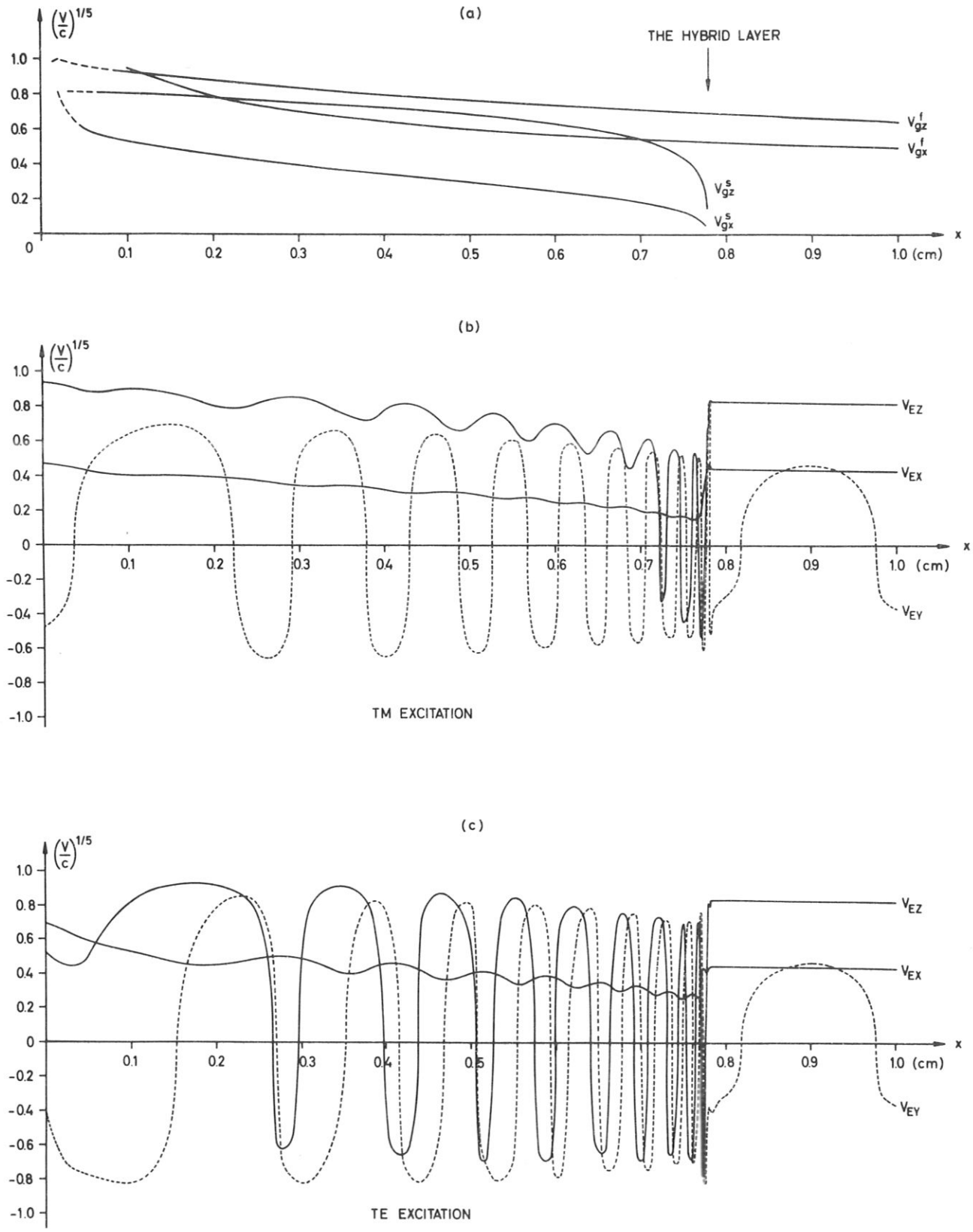
(a)
$\left(\frac{V}{c}\right)^{1/5}$
THE HYBRID LAYER
1.0
0.8
0.6
0.4
0.2
0
0.1
0.2
0.3
0.4
0.5
0.6
0.7
0.8
0.9
1.0 (cm)
x
V_{gz}^{f}
V_{gx}^{f}
V_{gz}^{s}
V_{gx}^{s}
(b)
$\left(\frac{V}{c}\right)^{1/5}$
V_{EZ}
V_{EX}
V_{EY}
-0.2
-0.4
-0.6
-0.8
-1.0
TM EXCITATION
(c)
$\left(\frac{V}{c}\right)^{1/5}$
V_{EZ}
V_{EX}
V_{EY}
TE EXCITATION

Fig. 18

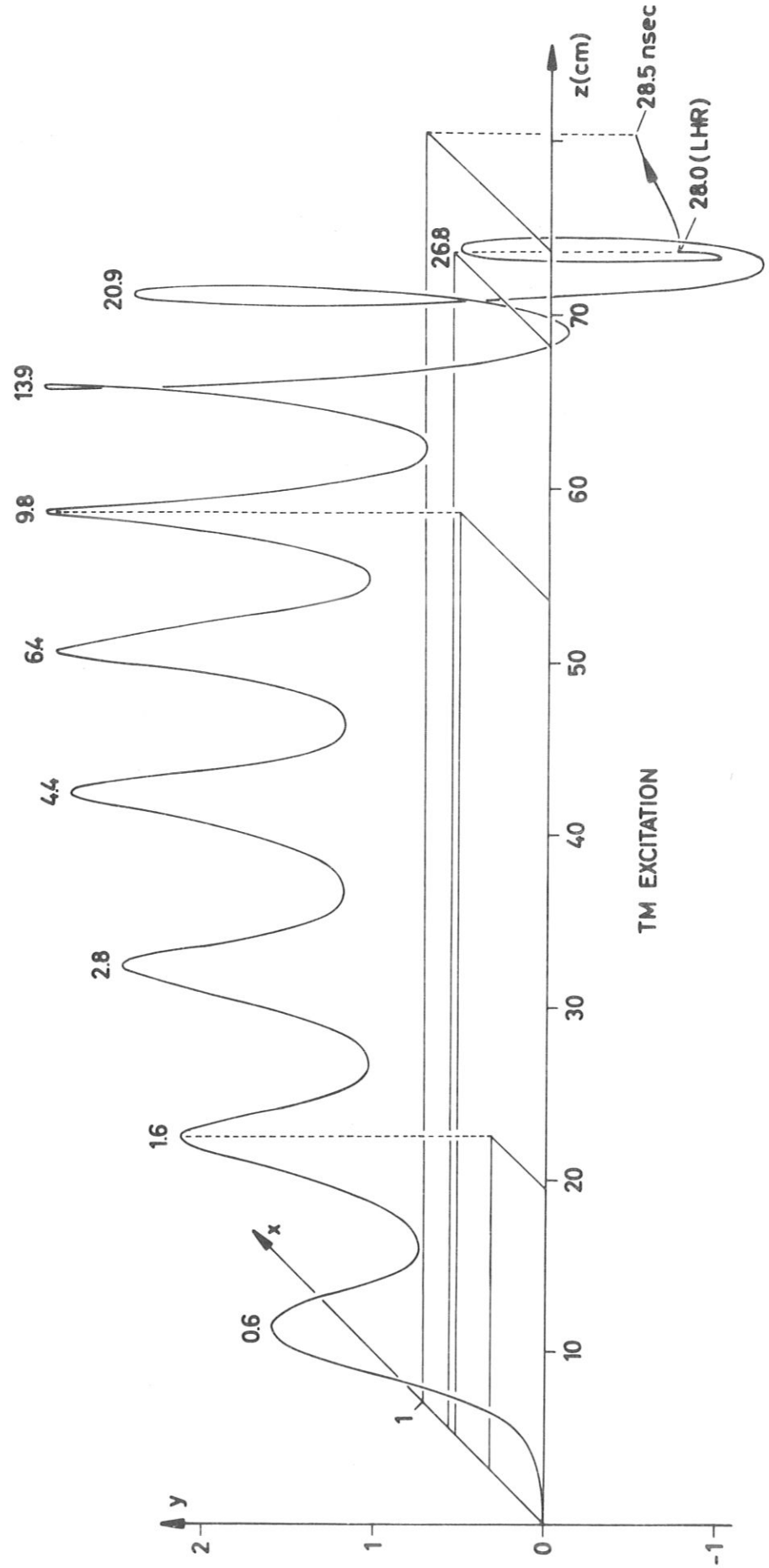
z(cm)
28.5 nsec
28.0 (LHR)
26.8
20.9
13.9
9.8
6.4
4.4
2.8
1.6
0.6
1
x
y
TM EXCITATION
70
60
50
40
30
20
10
0
2
1
-1

Fig. 19

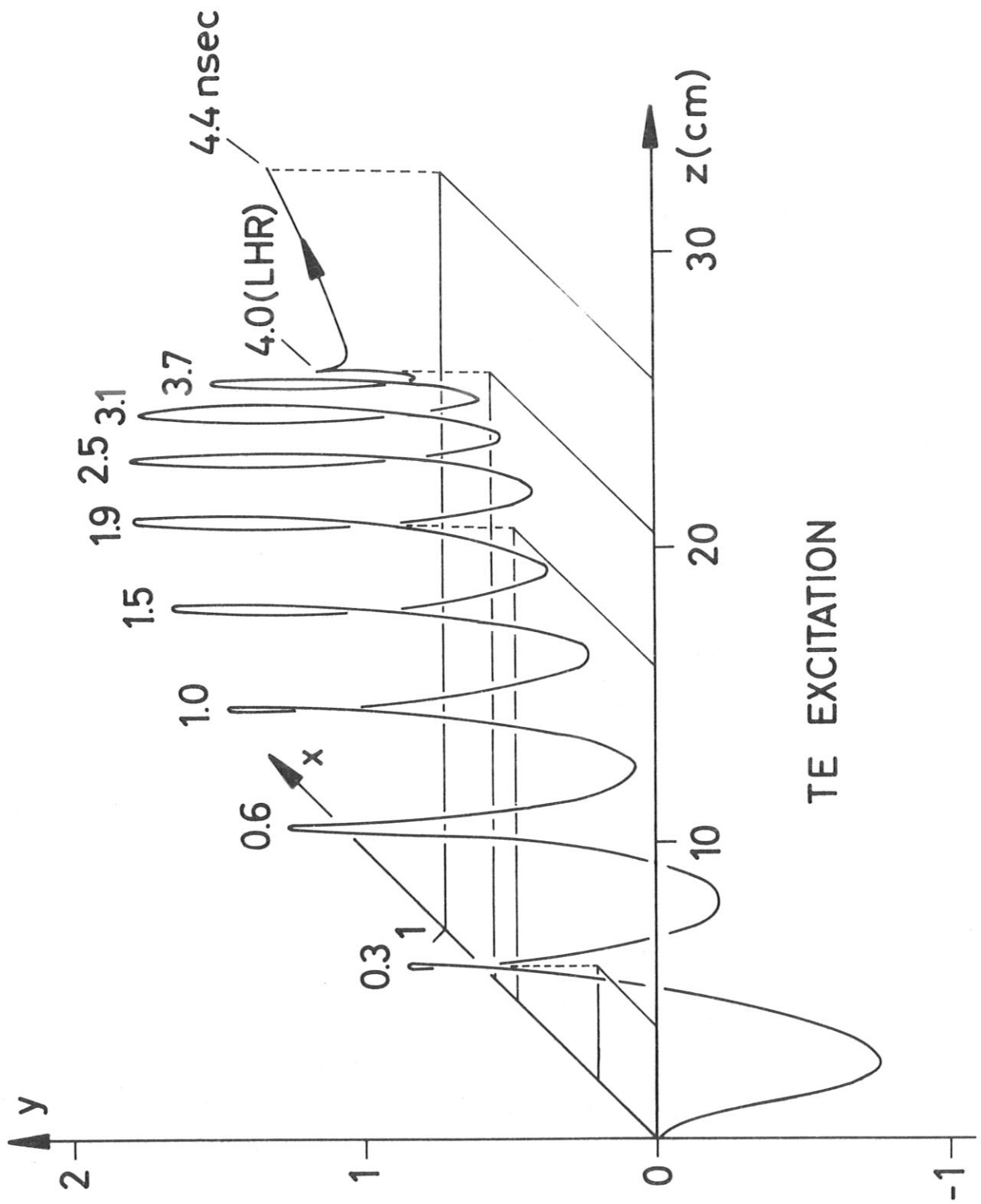
4.4 nsec
4.0(LHR)
3.7
3.1
2.5
1.9
1.5
1.0
0.6
0.3
1
x
y
z(cm)
30
20
10
2
1
0
-1
TE EXCITATION

Fig. 20

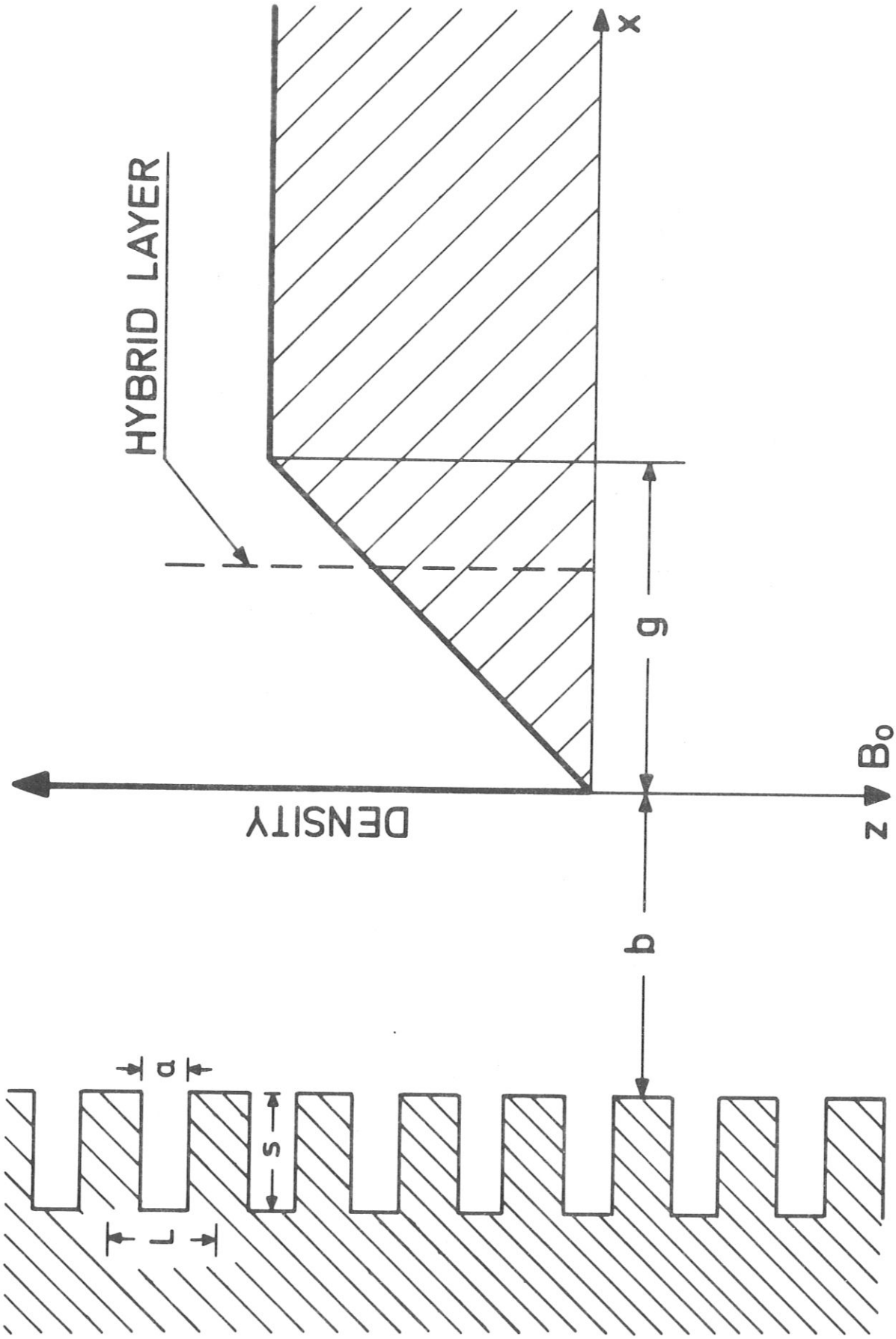

Fig. 21